Hall Anomaly, Quantum Oscillations and Possible Lifshitz Transitions in Kondo Insulator YbB$_{12}$: Evidence for Unconventional Charge Transport

Ziji Xiang[1,2,*] Kuan-Wen Chen,[1] Lu Chen,[1,§] Tomoya Asaba,[1,3] Yuki Sato,[3] Nan Zhang,[2] Dechen Zhang,[1] Yuichi Kasahara,[3] Fumitoshi Iga,[4] William A. Coniglio,[5] Yuji Matsuda,[3] John Singleton,[6,†] and Lu Li[1,‡]

[1]*Department of Physics, University of Michigan, Ann Arbor, Michigan 48109, USA*
[2]*CAS Key Laboratory of Strongly-coupled Quantum Matter Physics, Department of Physics,*
University of Science and Technology of China, Hefei, Anhui 230026, China
[3]*Department of Physics, Kyoto University, Kyoto 606-8502, Japan*
[4]*Institute of Quantum Beam Science, Graduate School of Science and Engineering,*
Ibaraki University, Mito 310-8512, Japan
[5]*National High Magnetic Field Laboratory, 1800 East Paul Dirac Drive,*
Tallahassee, Florida 32310-3706, USA
[6]*National High Magnetic Field Laboratory, MS E536, Los Alamos National Laboratory,*
Los Alamos, New Mexico 87545, USA

In correlated electronic systems, strong interactions and the interplay between different degrees of freedom may give rise to anomalous charge-transport properties, which can be tuned by external parameters like temperature and magnetic field. Recently, magnetic quantum oscillations and metallic low-temperature thermal conductivity have been observed in the Kondo insulator YbB$_{12}$, whose resistivity is a few orders of magnitude higher than those of conventional metals. As yet, these unusual observations are not fully understood. Here we present a detailed investigation of the behavior of YbB$_{12}$ under intense magnetic fields using both transport and torque magnetometry measurements. The Hall resistivity displays a strongly nonlinear field dependence which cannot be described using a standard two-band Drude model. A low-field Hall anomaly, reminiscent of the Hall response associated with "strange-metal" physics, develops at $T < 1.5$ K. At two characteristic magnetic fields ($\mu_0 H_1 = 19.6$ T and $\mu_0 H_2 \sim 31$ T), signatures appear in the Hall coefficient, magnetic torque, and magnetoresistance; the latter characteristic field coincides with the occurrence of a change in quantum-oscillation frequency. We suggest that they are likely to be field-induced Lifshitz transitions. Moreover, above 35 T, where the most pronounced quantum oscillations are detected, the background resistivity displays an unusual, nonmetallic T^α behavior, with α being field dependent and varying between -1.5 and -2 By normalizing the Shubnikov–de Haas oscillation amplitude to this T^α dependence, the calculated cyclotron mass becomes more consistent with that deduced from de Haas–van Alphen oscillations. Our results support a novel two-fluid scenario in YbB$_{12}$: A Fermi-liquid-like fluid of charge-neutral quasiparticles coexists with charge carriers that remain in a nonmetallic state. The former experience successive Lifshitz transitions and develop Landau quantization in applied magnetic fields, while scattering between both fluids allows the Shubnikov–de Haas effect to be observed in the electrical transport. The verification of this two-fluid scenario by the data in the current work strongly suggests that YbB$_{12}$ represents a new phase of matter.

---

[*]Corresponding author.
zijixiang@ustc.edu.cn
[†]Corresponding author.
jsingle@lanl.gov
[‡]Corresponding author.
luli@umich.edu
[§]Present address: Institut Quantique, Département de physique and RQMP, Université de Sherbrooke, Sherbrooke, Québec J1K 2R1, Canada.

I. INTRODUCTION

Kondo lattices are systems containing both conduction electrons (usually itinerant d electrons) and periodic arrays of local magnetic moments (typically localized f electrons). At low temperatures (T), interactions between these d and f bands lead to screening of the local moments, forming many-body states called Kondo resonances that in turn hybridize with the conduction-electron states [1]. This f-d hybridization opens a gap between the two hybridized quasiparticle bands that is centered on the energy level of the renormalized f states. If the conduction band is at exact half filling [2,3], or, more commonly, if the f states have a mixed valence [4], the Fermi energy lies within the hybridization gap, making the system a Kondo insulator (KI). Archetypal examples of KIs are cubic-structured f-electron compounds [5–7] SmB_6, YbB_{12}, and $Ce_3Bi_4Pt_3$. Thanks to the presence of strong electron correlations, the physical properties of these KIs are very unusual, differing significantly from those of conventional band insulators. For instance, the Kondo gap is usually quite narrow (most commonly 5–20 meV) and T dependent [5–7], exhibiting in-gap excitations even in the ground state [8,9]. In particular, the resistivity of KIs deviates from thermally activated behavior at temperatures of a few kelvins, below which the resistivity tends to saturate [6,10]. It is difficult to attribute these low-T resistive "plateaus" to conventional extended in-gap states because the large residual resistivity suggests unphysically short quasiparticle relaxation times [10]. Recently, theoretical works predicted time-reversal-invariant topological-insulator phases in some KIs with simple cubic structure [11–13]. Within such models, the low-T resistive plateau is taken as evidence for two-dimensional (2D) metallic transport channels associated with topological surface states. The proposed topological KIs attracted much theoretical and experimental interest, as they provide a new route toward the study of strongly correlated topological systems.

The most intensively studied KI is the mixed-valence compound SmB_6, which has a simple cubic lattice and is a candidate topological KI [14,15]. Numerous angle-resolved photoemission spectroscopy (ARPES) [16–21], scanning tunneling microscopy [22–24], planar tunneling spectroscopy [25,26], and electrical transport [27,28] experiments yield data supporting topological surface states in SmB_6. However, other experiments can be interpreted as not favoring the topological KI scenario [29,30]. The proposed topological nontriviality of other KIs is as yet inconclusive.

YbB_{12} crystallizes in a face-centered-cubic structure and also exhibits mixed-valence properties [6]; it is predicted to be a topological crystalline insulator that hosts surface states protected by the lattice symmetry [31]. However, while magnetotransport measurements confirm the contribution of surface transport channels [32], ARPES results suggest that the topological surface states are more

consistent with a strong topological insulator, rather than a topological crystalline insulator [33].

More intriguingly, unconventional magnetic quantum oscillations [34–37] and finite residual thermal conductivity $\kappa_{xx}/T(T \to 0)$ [38,39] attributable to three-dimensional (3D) fermionic states have been observed in both SmB_6 and YbB_{12}. Such observations are surprising since the two compounds exhibit $T \to 0$ resistivities that are at least 4 orders of magnitude higher than those of conventional metals; hence, extended electronic states (and therefore, a Fermi surface) are not expected. The case of SmB_6 is controversial, however, because the quantum oscillations [40–42] and the presence or absence of residual thermal conductivity [43,44] differ in single crystals grown by different techniques. Furthermore, only the de Haas–van Alphen (dHvA) effect (i.e., quantum oscillations in magnetization) has been reported in SmB_6, while the Shubnikov–de Haas (SdH) effect (i.e., quantum oscillations in electrical resistivity) has not been observed. All of these inconsistencies lead to doubts that the unconventional properties of SmB_6 are intrinsic [45].

Both SdH and dHvA oscillations are observed in YbB_{12}; these oscillations are well described by the Lifshitz-Kosevich (LK) formula that is appropriate for Fermi liquids. Moreover, the various extrinsic explanations for the observed phenomena can be excluded [35,36]. The Fermi-surface (FS) sections revealed by the quantum oscillations are 3D pockets containing quasiparticles with relatively large effective masses [35]; these are qualitatively consistent with the itinerant fermion contribution to the low-T thermal conductivity [39]. These results provoke a natural interpretation that the "insulating" bulk of YbB_{12} hosts exotic quasiparticles: They couple to magnetic fields and are able to carry thermal energy, but have a very weak response to electric fields. Recently, we discovered that the SdH effect of these unconventional fermions survives above the insulator-metal (I-M) transition at a magnetic field (H) higher than $\mu_0 H \approx 45$ T, yet changes its behavior in the high-field Kondo-metal (KM) state [36]. The complex behavior of YbB_{12} strongly suggests that the Landau quantization occurs in a band of charge-neutral quasiparticles which also give rise to the metallic κ_{xx} [36].

The presence of charge-neutral fermions in YbB_{12} suggests that, in addition to the postulated topological surface states, the bulk states of KIs are also unusual and may provide another approach to strongly correlated topological quantum matter. In a mean-field description of the Kondo lattice, the local moments can be fractionalized into multiplets of Majorana fermions, resulting in gapless 3D Majorana channels even in a charge-insulating ground state [46–49]. More recent theoretical works consider topologically protected gapless Majoranas that stem from the phase shifts of bands in mixed-valence insulators [50] or a Landau-Fermi-liquid ground state containing Majorana polarons in KIs [51]. In addition to the latter

proposals, other models propose spin-charge separation in mixed-valence materials [52–54]: Emergent neutral fermions that couple to a U(1) gauge field (similar to the spinons in quantum-spin liquids [55]) can appear in such a scenario and subsequently hybridize into fermionic composite excitons [53]. Given these competing theories of charge-neutral fermions, further experimental data are required to clarify the nature of the ground state in YbB_{12}. In particular, a key question to be addressed is how these charge-neutral fermions lead to the quantum oscillations in electrical transport properties.

In this work, we report a detailed study of the Hall effect, magnetoresistance (MR), and magnetic torque (τ) in high-quality single crystals of YbB_{12} in static magnetic fields of up to 45 T and pulsed magnetic fields of up to 55 T. Our main findings include the following.

(1) A low-field anomaly in the Hall resistivity ρ_{xy} appears at $T \lesssim 1.5$ K and becomes almost T independent for $T < 0.9$ K. This anomaly cannot be described by a two-band Drude model that takes into account surface conduction. However, it resembles the Hall response in strange metals without full quasiparticle coherence [56–58].

(2) Successive characteristic magnetic fields are indicated by features in ρ_{xy}, MR, and τ at $\mu_0 H = 19.6$ T and $\simeq 31$ T. We suggest these are signatures of putative field-induced Lifshitz transitions in the FS sections of the unconventional neutral quasiparticles.

(3) The SdH effect is observed in the field range 25.5 T $\leq \mu_0 H \leq 30$ T for the first time. The oscillations possess smaller frequencies but suggest cyclotron masses comparable to those associated with the SdH effect measured above 35 T [35,39]. This further supports the occurrence of electronic transition(s).

(4) The previously reported difference between the cyclotron masses extracted from dHvA and SdH data [35] can be partly resolved by considering the unusual T^α dependence ($\alpha < 0$) of the background resistivity in high magnetic fields. This T dependence suggests one or more novel scattering mechanisms in this system.

These results strongly imply that any "conventional" electrons and holes (i.e., charge carriers) in the KI state of YbB_{12}, either on the surface or in the bulk, form a possibly non-Fermi-liquid (non-FL) state that dominates the unusual transport behavior. By contrast, there is also a FL-like state of neutral qusiparticles that experience orbital quantization under magnetic fields. Consequently, the SdH effect appears through scattering between the neutral quasiparticles and the charged excitations. Such a scenario points to a unique two-fluid picture in YbB_{12} incorporating both emergent exotic excitations and potential strange-metal physics, as well as the interplay between them.

YbB_{12} is thus an ideal platform for investigating unusual many-body effects in condensed-matter physics.

II. METHODS

The single-crystal YbB_{12} samples are grown at the Ibaraki University using the floating-zone method [59]. Samples are cut from the ingots and polished into rectangular bar-shaped platelets with all surfaces normal to the [100] principal axes of the cubic lattice. Two batches of samples are measured here. The first batch includes samples $N1$ and $N2$, which are characterized in our previous works using quantum-oscillation and thermal-transport measurements [35,36,39]. The typical dimensions of these samples are $2.3 \times 1 \times 0.2$ mm^3 (length × width × thickness). The second batch, including samples Ha and Hb, has typical dimensions $2.5 \times 0.6 \times 0.1$ mm^3. No differences in physical properties are observed within each batch of samples. However, the behavior of the low-T resistivity differs slightly between the two batches (see the Appendix A).

The longitudinal resistivity ρ_{xx} and the Hall resistivity ρ_{xy} are measured simultaneously in a conventional six-probe Hall-bar configuration. Gold wires with diameter 25 μm are attached to the sample surface using Dupont 4922N silver paint, resulting in contact resistances of approximately 1 Ω. In pulsed-field Hall measurements, the contacts of the voltage leads are further secured by a small amount of Epo-Tek H20E silver epoxy for stability against mechanical vibrations during the pulses. Hall resistivity data are taken in three different cryostats: a dilution refrigerator in an 18-T superconducting magnet (SCM1) at the National High Magnetic Field Laboratory (NHMFL) in Tallahassee (sample $N2$), a Quantum Design DynaCool^{TM} 14-T system with ^{3}He insert (sample $N1$), and a ^{3}He cryostat in a capacitor-driven 65-T pulsed magnet at the NHMFL in Los Alamos (samples Ha and Hb). To remove stray ρ_{xx} contributions from the Hall voltage, ρ_{xy} is extracted using $\rho_{xy} = t[V_y(+H) - V_y(-H)]/2I_x$, where $(-H)$ and $(+H)$ indicate the values obtained on negative and positive field sweeps, and V_y and I are the measured voltage and applied electric current, respectively; t is the sample thickness. In the pulsed-field Hall experiments, this procedure is done separately for up and down sweeps of the field to eliminate possible effects of inductive (eddy-current) heating.

Torque magnetometry measurements are performed in magnetic fields of up to 45 T in the hybrid magnet at NHMFL, Tallahassee. The details of the procedures used are given in one of our earlier works [35].

III. THE LOW-FIELD HALL ANOMALY

A. The low-field Hall effect in YbB_{12}

Figure 1(a) shows $\rho_{xy}(H)$ for the YbB_{12} sample $N2$ at T's ranging from 20 to 841 mK measured at fields of up to
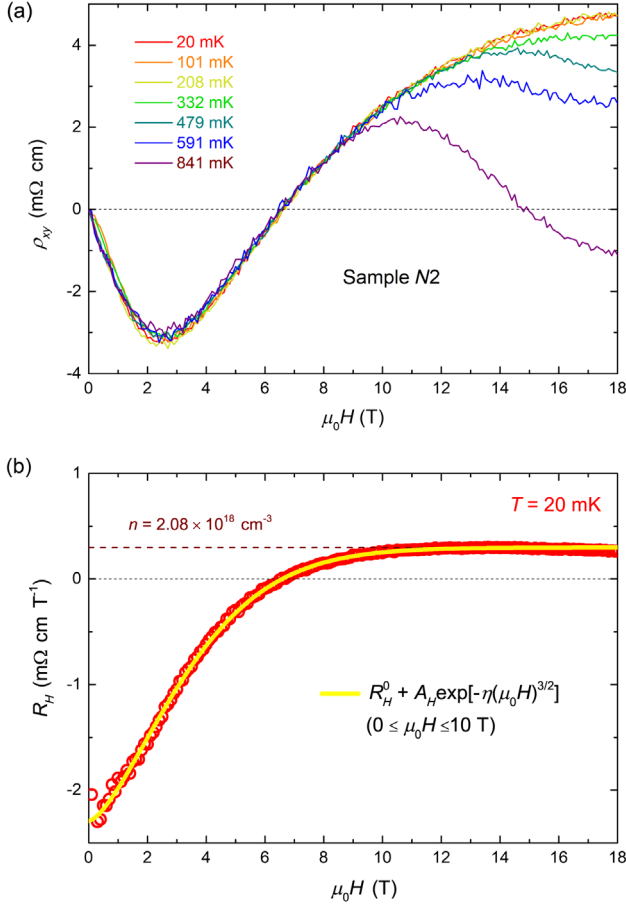
FIG. 1. (a) Hall resistivity ρ_{xy} of YbB$_{12}$ sample $N2$ measured in a dilution refrigerator in magnetic fields of up to 18 T. $\rho_{xy}(H)$ shows a sign change at $\mu_0 H \simeq 6.6$ T. Below this field, ρ_{xy} is negative and highly nonlinear with magnetic field, showing a low-field Hall anomaly which is nearly T independent from 20 to 841 mK. (b) Fitting of the field dependence of the Hall coefficient $R_H(H) \equiv \rho_{xy}(H)/(\mu_0 H)$ below 10 T using (yellow thick line) the empirical expression Eq. (1).

$\mu_0 H = 18$ T. The field dependence of ρ_{xy} is quite unlike those of conventional insulators or doped semiconductors. First, at these low T's, $\rho_{xy}(H)$ is almost T independent below 9T, suggesting that the low-T, low-H Hall effect is not primarily due to thermally activated charge carriers. Second, ρ_{xy} does not vary linearly with H. At low H, ρ_{xy} is negative (i.e., dominated by negative charge carriers); subsequently, following a minimum at approximately 2.6 T, it increases, changing sign at 6.6 T. Furthermore, at $T = 841$ mK, $\rho_{xy}(H)$ again changes sign (from positive to negative) at approximately 14.8 T. This behavior contrasts sharply with that in SmB$_6$ (where $\rho_{xy} \propto H$ [60]), and suggests a complicated multiband character for the low-field charge transport in YbB$_{12}$. Conventionally, such a field-dependent Hall effect would be understood in terms of a metal or semimetal with multiple electron and hole FS pockets. However, in YbB$_{12}$ the large, nonmetallic low-T

ρ_{xx} (Appendix A) and the strongly negative MR (Appendix B) preclude the existence of a bulk FS comprising charged quasiparticles. We discuss the validity of applying a conventional band-transport picture to YbB$_{12}$ Hall data in more detail in the Appendix C, where we show that the nonlinear ρ_{xy} displayed in Fig. 1(a) cannot be interpreted within the framework of a conventional two-band Drude model.

The unusual low-field behavior of the Hall effect (i.e., the initially negative ρ_{xy} with a minimum between 2 and 3 T and sign change at 6–7 T) is rapidly suppressed for $T \gtrsim 0.9$ K and completely disappears at $T = 2.5$ K [Fig. 2(a)]. At higher T, ρ_{xy} is negative with no sign change up to 14 T, but it is still not linear in H [Fig. 2(a)]. Such a nonlinearity is most apparent at higher magnetic fields and gradually becomes weaker upon warming, whereas a quasi-H-linear behavior shows up at low H [Fig. 2(b)]. The values of $\ln|\rho_{xy}|$ at $\mu_0 H = 1$ T are plotted against T^{-1} in Fig. 2(c); we extract the Kondo gap Δ by applying linear fits [via $\rho_{xy}(T) \propto n^{-1} \propto \exp(\Delta/2k_B T)$, where n is the carrier density and k_B the Boltzmann constant]. The fits suggest the presence of two different gaps with $\Delta_1 = 18.2 \pm 0.5$ meV between 50 and 17.5 K and $\Delta_2 = 3.2 \pm 0.5$ meV between 6 and 15 K. Similar two-gap behavior has been observed in previous transport studies of YbB$_{12}$ [59] and SmB$_6$ [30]; it is attributed to the complex level mixing in the hybridization process related to the crystal-field splitting of the $4f$ states [30,61,62]. The values of Δ_1 and Δ_2 deduced here are slightly different from those obtained from ρ_{xx} [35] but are consistent with those from earlier Hall measurements [59]. Therefore, in strong contrast to the situation below approximately 1 K [Fig. 1(a)], the low-field ρ_{xy} for $T > 6$ K seems to be dominated by the thermally activated carrier density n in YbB$_{12}$; it may be thought of as a reasonably conventional Hall effect with $\rho_{xy} = R_H \mu_0 H$, where $R_H = (ne)^{-1}$. On the other hand, the unusual low-H Hall behavior for $T < 1.5$ K shows that a thermal activation description is insufficient to account for all of the transport properties of YbB$_{12}$.

B. Origin of the Hall anomaly

The low-field Hall anomaly is observed in three YbB$_{12}$ samples from two different batches: sample $N1$ [Fig. 2(a)] and $N2$ [Fig. 1(a)] from batch 1 and sample Ha [Fig. 3(a)] from batch 2. The behavior of $\rho_{xy}(H)$ in these samples shows qualitative consistency, suggesting that the anomaly is an intrinsic property of YbB$_{12}$. We now discuss possible mechanisms and examine their validity in the context of our Hall data.

The anomalous Hall effect (AHE) often results in unusual Hall-effect data that do not scale linearly with H, especially at low magnetic fields. In ferromagnets, the conventional AHE is proportional to the magnetization M [63]. However, the $M(H)$ in YbB$_{12}$ [inset in Fig. 2(a)] is too
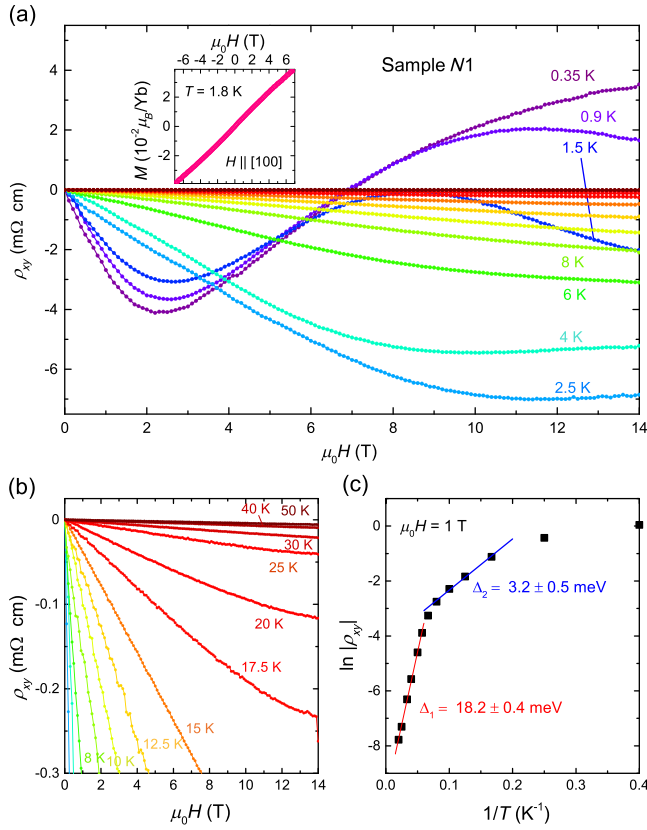
FIG. 2. (a) $\rho_{xy}(H)$ measured at temperatures ranging from 0.35 to 50 K in the YbB$_{12}$ sample $N1$ up to 14 T. The low-field anomaly becomes weaker above 0.9 K and completely disappears at 2.5 K. The negative Hall signal at higher temperatures indicates that electronlike carriers dominate. (Inset) Magnetization M of sample $N1$ versus magnetic field $H\|[100]$ ranging from -7 to $+7$ T at 1.8 K. The low-field $M(H)$ exhibits featureless and monotonic behavior. (b) Expanded view of the $\rho_{xy}(H)$ curves measured at $T > 15$ K. (c) Arrhenius plot: $\ln|\rho_{xy}|$ at $\mu_0 H = 1$ T plotted against $1/T$. The linear fits in the temperature ranges 20 K $\leq T \leq 50$ K and 6 K $\leq T \leq 12.5$ K yield Kondo gap widths $\Delta_1 = 18.2$ meV and $\Delta_2 = 3.2$ meV, respectively.

small to result in a significant AHE. Moreover, it does not exhibit any form of unusual field dependence that could be responsible for the strong curvature of the Hall data. [Note that the small size of $M(H)$ in YbB$_{12}$ comes from the fact that it is a KI, so that the Yb local moments are fully screened in the ground state.]

Recently, an "unconventional" AHE was proposed for nonmagnetic topological materials; this originates from nonzero Berry curvature in the vicinity of Weyl nodes or gapped band crossings [64,65]. For YbB$_{12}$, however, no such topological objects have been proposed for the band structure of YbB$_{12}$. Moreover, even if they dominate the electrical transport, topological surface states should not exhibit an AHE in the absence of magnetism.

In many heavy-fermion compounds, there is a third type of AHE that results from skew scattering: In magnetic fields, the conduction electrons are scattered asymmetrically by the magnetic moments of the f electrons [32,66]. Though this effect can contribute a large portion of the measured Hall signal, this usually occurs at high T, where the localized f electrons are not fully screened so that they can act as scattering centers [67]. At very low T, the skew-scattering effect involves only residual impurities; consequently, the corresponding AHE becomes rather weak compared to the conventional Hall effect [68–70]. Moreover, most of the models of the AHE in heavy-fermion systems predict $R_H \propto \chi$ [71], where $\chi = M/H$ is the magnetic susceptibility. This is nearly H independent [inset of Fig. 2(a)] in YbB$_{12}$. Therefore, skew-scattering-induced AHE can be excluded as the origin of the H-nonlinear Hall anomaly in YbB$_{12}$.

In the low-field limit ($\mu H \ll 1$ T, here μ is the carrier mobility), the Hall coefficient can be severely affected by details of the quasiparticle scattering; it thereby deviates from simple relationships such as, e.g., $R_H = 1/ne$ [72]. It is well known that in 2D electron systems, such as the surface states in YbB$_{12}$, the amplitude and even the sign of the low-field Hall effect depend on the geometry (local curvature) of the FS [73]. Nevertheless, ARPES data suggest a single Fermi contour at the center of the surface Brillouin zone with no apparent anisotropic curvature [33]. Therefore, the FS geometry arguments are perhaps irrelevant here. Alternatively, anisotropic scattering can stem from antiferromagnetic (AFM) fluctuations with certain wave vectors [74,75]. We remark that in YbB$_{12}$, the presence of dispersive in-gap spin excitons due to short-range AFM correlations has been confirmed [76,77]. In particular, the presumably reduced strength of Kondo coupling at the surface can give rise to enhanced AFM stabilities and even push the system toward quantum criticality [78]; spin-exciton-mediated scattering naturally provides strong anisotropic scattering channels for the surface quasiparticle states.

While it seems that most of the established models do not account for the Hall anomaly in YbB$_{12}$, we stress that this feature can be almost perfectly fitted by an empirical expression [yellow line in Fig. 1(b)]:

$$R_H = R_H^0 + A_H \exp[-\eta(\mu_0 H)^{\frac{3}{2}}]. \tag{1}$$

Here, R_H^0 is a field-independent term with the value 0.3 mΩ cm T^{-1}, and $A_H \exp[-\eta(\mu_0 H)^{\frac{3}{2}}]$ is the "anomalous" term that gives rise to the nonlinear behavior, with A_H and η being fitting parameters. Significantly, a similar Hall enhancement at low H has been observed in the "strange-metal" phase of iron-based superconductors BaFe$_2$(As$_{1-x}$P$_x$)$_2$ [57] and FeSe$_{1-x}$S$_x$ [58]. In both cases, the enhancement is also $\propto \exp[-\eta(\mu_0 H)^{\beta}]$ with the exponents $\beta = 1$ for BaFe$_2$(As$_{1-x}$P$_x$)$_2$ [57] and $\beta = 2$ for FeSe$_{1-x}$S$_x$ [58]. In both iron-based superconductors, the strange-metal state is related to the proximity to a

putative quantum-critical point (QCP) [a pure nematic QCP in $FeSe_{1-x}S_x$ [58,79] and a (mainly) AFM QCP in $BaFe_2(As_{1-x}P_x)_2$ [80,81]]. Hence, the successful fit to Eq. (1) with $\beta = 3/2$ strongly suggests a strange-metal state in YbB_{12}, and it would be of interest to explore whether critical magnetic instabilities, possibly induced by the weakened Kondo coupling at the surface [78], contribute to the formation of such states.

The two terms in Eq. (1) represent a strange-metal contribution $A_H \exp[-\eta(\mu_0 H)^{\frac{3}{2}}]$ plus a constant R_H^0. If one for a moment assumes R_H^0 to be the conventional part of the Hall effect, it corresponds to a rather high carrier density $n \simeq 2.08 \times 10^{18}$ cm^{-3} (equivalent to $n^{2D} \simeq 4.4 \times 10^{16}$ cm^{-2}). This means R_H^0 cannot be interpreted as due to a conventional band contribution. Such a heavily modified apparent n could be the consequence of emergent quasi-particle decoherence, as reported in the strange-metal regime of cuprate high-T_c superconductors [56]. Thus, it seems that the low-T, low-H R_H in YbB_{12} is dominated entirely by strange-metal physics. Since the low-T, low-H electrical conduction in YbB_{12} is thought to be due to the surface channel [32], the strange-metal state likely resides on the surface, where the quasiparticles lose coherence through scattering from abundant bulk excitations. We further discuss this in Sec. VI.

IV. EVIDENCE FOR FIELD-INDUCED LIFSHITZ TRANSITIONS

A. Hall resistivity at high magnetic field

With increasing H, the electrical transport in YbB_{12} exhibits a crossover from the low-field surface-dominated regime to the high-field bulk-conducting regime [32] where quantum oscillations of 3D unconventional, charge-neutral fermions have been detected [35]. The behavior of $\rho_{xy}(H)$ is in agreement with this picture. As displayed in Fig. 3(b),

at $T = 0.56$ K, the positive ρ_{xy} developed above the sign change around 7 T [Fig. 3(a)] is slowly suppressed, leading to a second sign change from positive to negative at approximately 20 T. For $\mu_0 H \gtrsim 20$ T, ρ_{xy} appears to be electronlike all the way up to the I-M transition field H_{I-M} [$\mu_0 H_{I-M} = 46.6$ T for samples Ha and Hb; Fig. 3(c)]; this is identified as the contribution of bulk carriers. The minimum (i.e., the largest magnitude negative value) $\rho_{xy} \approx -2.5$ mΩ cm occurs at approximately 35 T [Fig. 3(c)]. In the field-induced KM state ($H > H_{I-M}$) [82] the Hall signal drops below our experimental resolution.

The measurement of tiny Hall signals in pulsed magnetic fields is affected by issues such as eddy-current heating (due to large field-sweeping rate), the magneto-caloric effect, and induced-voltage pickup in the circuit. In the present case, difficulties may arise because the longitudinal resistivity in YbB_{12} is both large ($\rho_{xx}/\rho_{xy} > 100$ over the entire field range) and very T dependent [35]. Hence, an exact, quantitative extraction of the Hall voltage using a comparison of positive and negative field sweeps depends on T being identical throughout both pulses. A slight mismatch in T is likely responsible for the difference between the data recorded on the up and down sweeps of the field in Fig. 3(c). While the magnitudes of the ρ_{xy} signals shown in Fig. 3(c) should therefore be treated with caution, it is clear that two noticeable signatures in the high-field ρ_{xy} curves are very consistently observed and therefore very likely to be intrinsic. These are two sharp slope changes at approximately 20 T (i.e., near the second sign change) and approximately 30 T marked by gray vertical bars in Fig. 3(c). As we discuss in detail in the following sections, we propose that these features are likely to signify field-induced Lifshitz transitions, i.e., electronic topological transitions that describe changes in the FS topology [83].
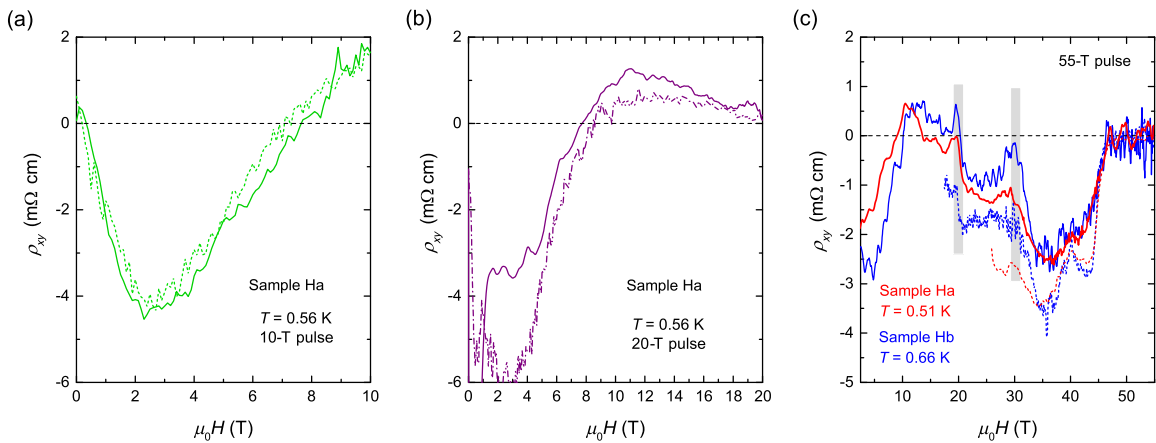

FIG. 3.   Field dependence of Hall resistivity in YbB_{12} measured in pulsed magnetic fields for (a) sample Ha at 0.56 K up to 10 T, (b) sample Ha at 0.56 K up to 20 T, (c) sample Ha at 0.51 K, and sample Hb at 0.66 K in magnetic fields of up to 55 T. Solid and short-dashed lines are field up sweeps and down sweeps, respectively. The $\rho_{xy}(H)$ curves are obtained by subtracting the negative from the positive field sweeps. The two light gray bars in (c) mark the fields corresponding to possible Lifshitz transitions.
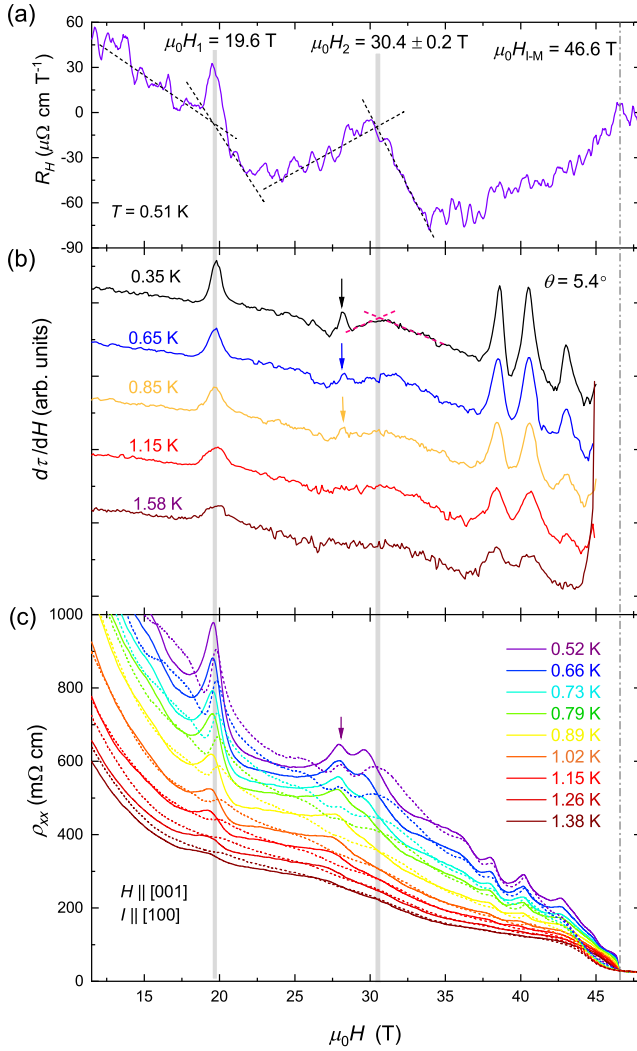
FIG. 4. Comparison of the field dependence of (a) Hall coefficient R_H, (b) field derivative of the magnetic torque $d\tau/dH$ taken with tilt angle $\theta = 5.4°$ between H and the [001] direction and (c) transverse resistivity ρ_{xx} versus H applied along the [001] direction in YbB$_{12}$. The insulator-to-metal-transition field $\mu_0 H_{\text{I–M}}$ is 46.6 T in this sample, as denoted by the vertical dash-dotted line. Clear dHvA and SdH oscillations appear below $H_{\text{I–M}}$ as shown in (b) and (c), respectively. The vertical gray thick lines represent two characteristic fields: a nearly T-independent signature $\mu_0 H_1 = 19.6$ T manifested by (a) a slope change in R_H and peaks in (b) $d\tau/dH$ and (c) $\rho_{xx}(H)$, and a second signature occurring at $\mu_0 H_2 = 30.4 \pm 0.2$ T which is implied by the kinks in R_H and $d\tau/dH$ [dashed lines in (a) and (b), respectively]. This latter feature roughly corresponds to a local maximum in MR for the down sweeps. Alternatively, the small cusp in $d\tau/dH$ at approximately 28 T (arrows) is identified as an extremum of quantum oscillations (see Fig. 12 and Appendix D).

B. Comparison with the features in magnetic torque and magnetoresistance

Figure 4 shows the field dependence of the Hall coefficient R_H [Fig. 4(a)], the derivative of the magnetic torque $d\tau/dH$ [Fig. 4(b)], and $\rho_{xx}(H)$ [Fig. 4(c)] measured

in the YbB$_{12}$ sample Ha. Several signatures show up in all three quantities. At $\mu_0 H_1 = 19.6$ T, a kink (slope change) is observed in R_H [indicated by the dashed lines in Fig. 4(a)]. (Note that the peak at $H \approx H_1$ may be caused by a slightly incomplete cancellation of the picked-up ρ_{xx} terms between the negative and positive field sweeps due to small temperature difference.) At the same field, strong peaks occur in both $d\tau/dH$ and ρ_{xx}. The features at H_1 gradually smear out at higher T, yet the characteristic field H_1 is almost T independent. At around 28 T, a small cusp appears in $d\tau/dH$ [arrow in Fig. 4(b)]. It approximately aligns with a local maximum in both field up sweeps and down sweeps of MR at temperatures below approximately 1 K [Fig. 4(c)]. We attribute this feature to an extremum of the quantum oscillation occurring between 25.5 and 30 T (Appendix D), which is further introduced in Sec. VA. Both R_H and $d\tau/dH$ show another kink [crossing of the two dashed lines in Figs. 4(a) and 4(b), respectively] at $\simeq 30.4$ T with the uncertainty of about 0.2 T; this feature identified as a second characteristic field H_2 is in line with a rounded maximum in the down sweeps of MR. All the signatures mentioned above are reproduced in the measurements of sample $N1$ (from a different batch), wherein the characteristic field H_1 stays unchanged but $\mu_0 H_2 = 31.3$ T is slightly higher (Appendix D).

Some of the signatures we present here were explained as field-induced metamagnetic transitions in our earlier work [35]. These attributions followed theoretical predictions that an AFM state will appear in KIs subjected to large magnetic fields that are below the gap closure [84,85]. However, it was later shown that the corresponding features are not observed in thermodynamic quantities such as the magnetocaloric effect [82], magnetostriction, and M [36]. In particular, the absence of a signature in M strongly suggests that they are not metamagnetic transition fields.

Instead, the signatures at the characteristic fields in YbB$_{12}$ closely resemble those in the heavy-fermion metal CeIrIn$_5$, where kinks in τ can be resolved but no feature appears in M. The latter kinks are interpreted as field-induced Lifshitz transitions that are not accompanied by metamagnetic transitions [86]: The modification in FS topology causes a change in the transverse magnetization (which is captured in τ) but has very weak impact on the longitudinal magnetization M. Although in numerous heavy-fermion materials the Zeeman-driven Lifshitz transition does correspond to a simultaneous metamagnetic transition [87], this does not happen in CeIrIn$_5$ due to the robustness of Kondo physics in this material against magnetic fields [86]. Such an argument will also be valid in YbB$_{12}$, where the field suppression of the Kondo gap cannot be understood as the destruction of Kondo correlation [36,82]. Consequently, we assign the characteristic fields shown in Figs. 4 and 12 to putative Lifshitz transitions (here we note that, whereas these transitions are likely to correspond to changes in FS topology, we do

not have strong evidence that they are of the order-$2\frac{1}{2}$ nature as for the rigorously defined Lifshihtz transitions [83]).

Further evidence for the possible Lifshitz transitions comes from the transport measurements: It is well known that Lifshitz transitions often yield kinks in the Hall effect and MR [69,88,89]. Whereas Lifshitz transitions may cause small changes in the field evolution of the density of states (DOS), which produce only weak signatures in thermodynamic quantities, they can correspond to the appearance or vanishing of scattering channels, strongly modifying the transport behaviors. Considering two basic types of Lifshitz transitions, namely, the FS "neck-breaking" and "void-creation" transitions, a simple model predicts that they are manifested by local maxima and minima of the electrical resistivity, respectively [89]. Following this idea, all of the putative Lifshitz transitions in YbB$_{12}$ are presumably of the neck-breaking type. In particular, the feature observed at H_2 may be interpreted as a Lifshitz transition that barely changes the DOS and is thus not obvious in τ [Fig. 4(b)]. Further information about the quasiparticle scattering is needed to pin down the details of the Lifshitz transitions. In this context, thermopower measurements under high magnetic fields [88] may be of great importance.

Perhaps the most direct verification of a Lifshitz transition is a discontinuity in the quantum-oscillation frequency, as has been observed, e.g., in CeIrIn$_5$ [86], YbRh$_2$Si$_2$ [90], and CeRu$_2$Si$_2$ [91]. In Sec. V A, we show that the SdH frequency changes drastically within the approximate field range 30–33 T. This strongly supports the occurrence of a Lifshitz transition in the corresponding field window, and it is tempting to assign it to the characteristic field H_2.

Given the nonmetallic transport behavior for $H < H_{\text{I–M}}$ in YbB$_{12}$, an important question is "what kind of Fermi surface plays host to the Lifshitz transitions?" As we discuss further in Sec. VI, a reasonable hypothesis is that the Lifshitz transitions occur in the FS of charge-neutral quasiparticles [36] and show up in the charge transport via interband scattering between the neutral quasiparticles and any conventional charge-carrying electrons. At this point, without knowing the exact form of the neutral-quasiparticle bands, we cannot provide a detailed scenario for the possible Lifshitz transitions. However, it is likely that they involve abrupt modifications of the neutral FSs that are triggered by the field-induced gap narrowing (see Sec. VI D).

V. QUANTUM OSCILLATIONS IN THE KI STATE

A. SdH effect in the field range 25.5 T $\leq \mu_0 H \leq$ 30 T

We previously reported dHvA and SdH oscillations in the KI state ($H < H_{\text{I–M}}$) of YbB$_{12}$ at magnetic fields $\mu_0 H \gtrsim$ 33–35 T [35,39]. Here we show that SdH oscillations actually emerge at lower H. As plotted in Fig. 4(c), $\rho_{xx}(H)$ traces recorded on the down sweeps of H (short-dashed lines) exhibit a double-dip feature in the field range 25.5 T $\leq \mu_0 H \leq$ 30 T. This feature is most evident at low T, gradually fading upon warming. While it is relatively clearer in sample Ha [Fig. 4(c)], this feature is also present in other batches of samples [see the shaded region in the inset of Fig. 12(c) and Appendix D]; it was simply overlooked in our earlier studies.

Figures 5(a) and 5(b) show the oscillatory component of ρ_{xx}, ρ_{xx}^{osc}, obtained using polynomial background
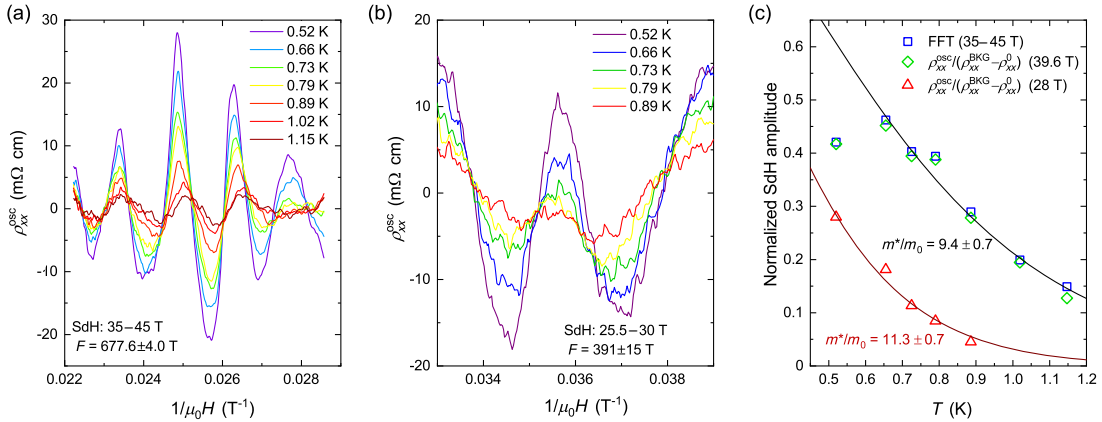

FIG. 5. The amplitude of the oscillatory component of resistivity ρ_{xx}^{osc} at various temperatures in the field ranges (a) $35 \leq \mu_0 H \leq 45$ T and (b) $25.5 \leq \mu_0 H \leq 30$ T. ρ_{xx}^{osc} is obtained by background subtraction of a polynomial from the $\rho_{xx}(H)$ curves shown in Fig. 4(c). The oscillation frequencies are mentioned in each panel. Note that for the field range displayed in (a), the oscillations have a single frequency which is supported by the dHvA measurements (see Supplemental Material, Figs. 1(a) and 1(b) [93]). (c) Lifshitz-Kosevich fits of the T dependence of ρ_{xx}^{osc} shown in (a) (green diamonds) and (b) (red triangles) normalized by the power-law T-dependent background resistivity (see Sec. V C for details). The temperature dependence of the FFT peak height (the FFT is performed after normalizing ρ_{xx}^{osc} by the background resistivity) of the oscillations shown in (a) (blue squares) is consistent with that of normalized ρ_{xx}^{osc}. All data are measured on sample Ha.

subtraction for $35 \text{ T} \leq \mu_0 H \leq 45 \text{ T}$ and $25.5 \text{ T} \leq \mu_0 H \leq 30 \text{ T}$, respectively. For both field ranges, the amplitudes of the oscillations shrink with increasing T in a similar way. In Fig. 5(c), we plot the T dependence of the normalized amplitude of the SdH effect and fit it using the LK formula [92]

$$\rho_{xx}^{\text{osc}}(T) \propto \frac{\frac{2\pi^2 k_B m^* T}{e\hbar\mu_0 H}}{\sinh\left(\frac{2\pi^2 k_B m^* T}{e\hbar\mu_0 H}\right)}, \qquad (2)$$

where m^* is the cyclotron mass for motion in the plane perpendicular to the applied H. (We note that to obtain reliable cyclotron masses, ρ_{xx}^{osc} must be normalized by the background resistivity before applying the LK fits; see Sec. V C.)

It appears that the LK formula [solid lines in Fig. 5(c)] describes the oscillation amplitudes well except for the lowest temperature point for the $35 \text{ T} \leq \mu_0 H \leq 45 \text{ T}$ data (this point is affected by the change of background resistivity behavior for $T \lesssim 0.5 \text{ K}$). Interestingly, while the fast Fourier transform (FFT) gives SdH frequencies $F = 678 \pm 4.0 \text{ T}$ and $391 \pm 15 \text{ T}$ for $35 \text{ T} \leq \mu_0 H \leq 45 \text{ T}$ and $25.5 \text{ T} \leq \mu_0 H \leq 30 \text{ T}$, respectively, the LK fits yield comparable cyclotron masses ($9.4 m_0$ and $11.3 m_0$, respectively, where m_0 is the mass of the free electron) for the two field regions. The similarity of the masses excludes magnetic breakdown as an explanation for the frequency change, which predicts that the mass of the large breakdown orbits equals the sum of the masses of the involved small orbits [based on the relation $m^* \propto (\partial S/\partial\epsilon)|_{\epsilon=E_F}$, where S, ϵ, and E_F are the orbit area, the energy, and the Fermi level, respectively] [92]. The consistency of the mass instead suggests that all of the SdH oscillations may originate from the same quasiparticle band(s), while a Lifshitz transition between the two field regions changes the extremal orbit area. This Lifshitz transition may be associated with the characteristic field H_2 in Fig. 4. Unfortunately, the SdH effect occurring below approximately 31 T is seen only in the down-sweep MR curves, and no more than one and a half periods are resolved. The hysteresis between the up and down sweeps of H suggests that these SdH oscillations may be associated with "metastable" states that are induced by and/or persist only over the ms timescales of the pulsed magnetic fields.

B. Nonmetallic transport at high fields

To further understand the SdH effect observed in the KI state of YbB$_{12}$, we investigate the T dependence of the nonoscillatory resistive background ρ_{xx}^{BKG} (i.e., the H-polynomial term which is subtracted from the raw MR data to get ρ_{xx}^{osc}) over the field range where the SdH oscillations are apparent (35–45 T). As displayed in Figs. 6(a) and 6(b), over a field-dependent T range, ρ_{xx}^{BKG} in sample N2 follows an unusual T^α behavior, with
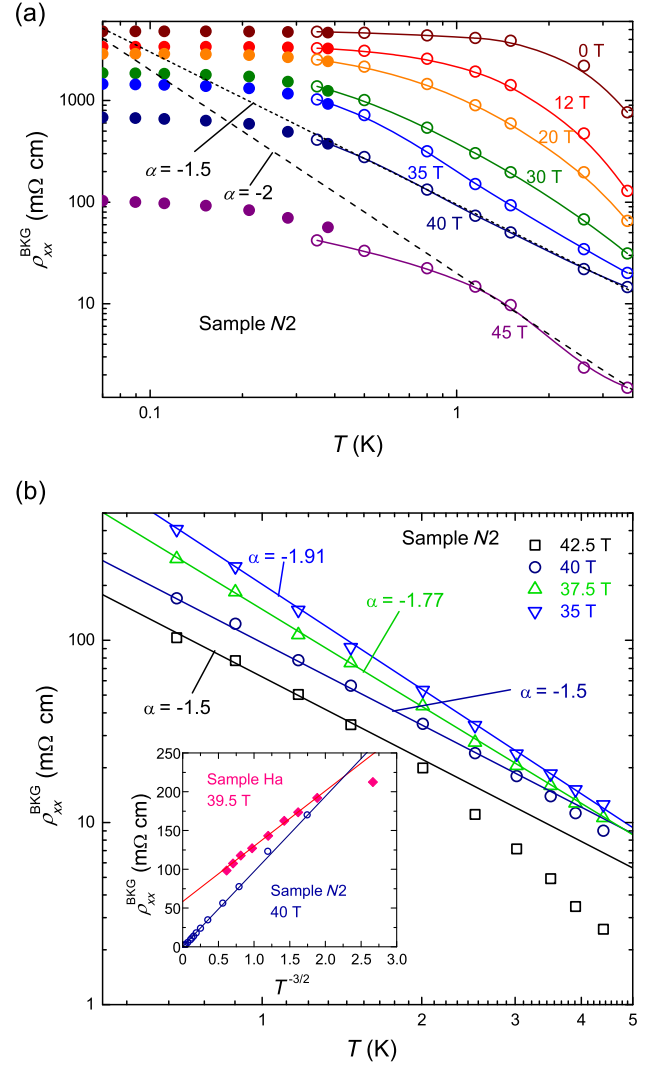

FIG. 6. (a) The nonoscillatory background resistivity ρ_{xx}^{BKG} of YbB$_{12}$ sample N2 as a function of the temperature at several magnetic fields from 0 to 45 T, plotted on a log-log scale. Open and solid symbols are data taken in the ^{3}He cryostat at magnetic field tilt angle $\theta = 7.4°$ and in the dilution refrigerator at $\theta = 8.5°$ in the 45-T hybrid magnet [35]. Solid lines are guides to the eye. Dashed and dotted lines denote $\rho_{xx} \propto T^\alpha$ with $\alpha = -2$ and $\alpha = -1.5$, respectively. (b) $\rho_{xx}^{\text{BKG}}(T)$ of sample N2 at $\mu_0 H = 35 \text{ T}$ (down triangles), 37.5 T (up triangles), 40 T (circles), and 42.5 T (squares) measured in a pulsed magnet with H applied along [001]. Solid lines indicate the power-law T dependence $\rho_{xx}^{\text{BKG}}(T) = A(H)T^\alpha$. (Inset) ρ_{xx}^{BKG} plotted against $T^{-3/2}$ for sample N2 ($\mu_0 H = 40 \text{ T}$) and Ha ($\mu_0 H = 39.5 \text{ T}$).

the exponent $\alpha < 0$ between 35 and 45 T. At 35 and 37.5 T, ρ_{xx}^{BKG} is well described by T^α functions for $0.5 \lesssim T \lesssim 5 \text{ K}$ with $\alpha = -1.91$ and -1.77, respectively [Fig. 6(b)]. For $\mu_0 H = 40 \text{ T}$, and $0.35 \lesssim T \lesssim 3 \text{ K}$, ρ_{xx} shows a perfect $T^{-1.5}$ dependence. On increasing the field to 42.5 T, $\alpha = -1.5$ is still valid but only for $T \lesssim 2 \text{ K}$ [Fig. 6(b)]. At 45 T (i.e., close to the I-M transition) a T^{-2} behavior emerges over a narrow T range above 1 K [Fig. 6(a)].

While the background resistivities in samples *N*2 and Ha can be fitted to the simple relationship $\rho_{xx}^{\mathrm{BKG}}(T) = \rho_{xx}^0 + A(H)T^\alpha$, the fitting parameters ρ_{xx}^0 and A are sample dependent. In particular, ρ_{xx}^0 is infinitesimal for sample *N*2, yet takes a value approximately equal to 60 mΩ cm in sample Ha [inset of Fig. 6(b)].

The T^α behavior with $-2.0 \lesssim \alpha \lesssim -1.5$ is strong evidence for nonmetallic charge transport upon which the SdH effect emerges. This behavior contrasts sharply with that of conventional SdH oscillations associated with a FL state. The underlying physics leading to the negative α is elusive at present. Theoretically, a $\rho \propto T^{-\frac{3}{2}}$ dependence can be attributed to ionized impurity scattering in nondegenerate semiconductors [94] or electron-phonon-dominated inelastic scattering in heavily disordered systems [95]. Neither electronic system is expected to produce quantum oscillations on its own.

More unusual, recent works on electrical transport in topological semimetals with small Fermi energies and charged impurities also predict $\rho \propto T^\alpha$ (with $\alpha < 0$) [96–98]. Indeed, it has been suggested that in KIs, impurity scattering leads to non-Hermitian in-gap states that effectively close the Kondo gap and turn the system into a nodal semimetal [99,100]. Although we later show that this does not happen in YbB$_{12}$ at $H = 0$ (see Appendix A), it is not clear whether it is relevant at high H, where the gap width is reduced. Whereas a T^{-1} dependence is predicted when only the thermal excitation of carriers across the nodal cone is taken into account [100], $\rho \propto T^{-4}$ is obtained if the T dependence of the scattering rate and thermal screening of impurities are included [96,97]. The exponent $-2.0 \lesssim \alpha \lesssim -1.5$ may therefore represent vestiges of these effects; for instance, the putative T^{-4} behavior is predicted to evolve [97] into a weakly-T-dependent "residual" resistivity at low T, qualitatively consistent with our observations for $T \lesssim 0.3$ K [Fig. 6(a)]. However, in proposed Weyl semimetals with small Fermi energies such as the iridate pyrochlores [101,102], a low-T saturation of ρ is experimentally absent.

C. Correction of the SdH amplitudes

Earlier works describing quantum oscillations in the KI state of YbB$_{12}$ noted an apparent contradiction; the cyclotron mass determined from the SdH effect $(14$–$15m_0)$ was much heavier than that obtained from dHvA oscillations $(6.5$–$7m_0)$ [35]. The discrepancy may now be understood as follows. Whereas the thermal damping of the dHvA oscillations is due only to phase smearing caused by the T-dependent broadening of the Fermi-Dirac distribution function [LK formula, Eq. (2)], SdH oscillations in electrical transport represent an additional convolution of this effect with the background resistivity. The latter will be affected by T-dependent scattering rates, an effect parametrized via $\nu \simeq \zeta(T)\tilde{g}$ [103], where ν is the scattering rate (inverse relaxation time), $\tilde{g}$ is the (T-independent) DOS,

and $\zeta(T)$ describes the T-dependent scattering processes. It is clear that $\zeta(T)$ should contribute equally to the oscillatory and nonoscillatory (background) components of the resistivity, so that $\rho^{\mathrm{osc}}(T)$ must be normalized by dividing by $\rho^{\mathrm{BKG}}(T)$ before fitting to the LK formula [104,105].

In our earlier work, $\rho_{xx}^{\mathrm{osc}}(T)$ was normalized in the traditional manner [103] using the zero-field resistivity
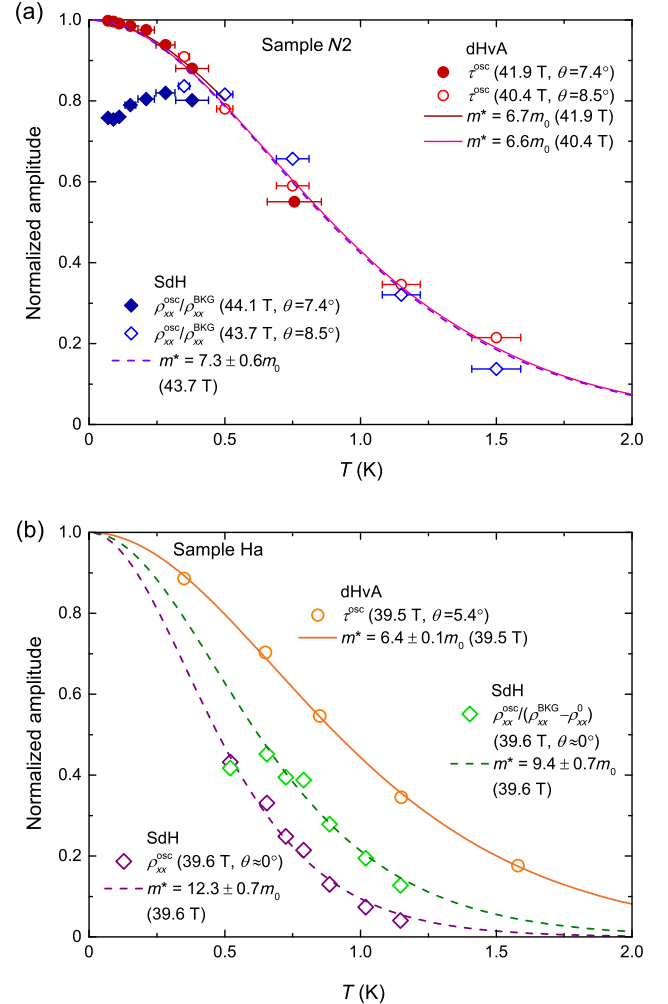

FIG. 7. Normalized quantum-oscillation amplitudes versus temperature for (a) sample *N*2 and (b) sample Ha. The dHvA amplitude τ^{osc} is obtained by subtracting a polynomial background from the magnetic torque $\tau(H)$ [35]. For sample *N*2, the SdH amplitude is taken as $\rho_{xx}^{\mathrm{osc}}/\rho_{xx}^{\mathrm{BKG}}$, i.e., the oscillatory part of resistivity ρ_{xx}^{osc} divided by the nonoscillatory background at the corresponding magnetic field. For sample Ha, a T-independent component ρ_{xx}^0 is further removed from the nonoscillatory resistivity background ρ_{xx}^{BKG} (see text). The absolute ρ_{xx}^{osc} without normalization using the background resistivity (purple diamonds) is also shown for comparison. Solid and dashed lines are fits to the LK formula for dHvA and SdH amplitudes, respectively. The inferred effective masses are shown beside the fits. Note that all the nonmonotonic T dependence of the SdH amplitudes are caused by the normalization; see the raw data presented in Supplemental Material Fig. 1(c) [93].

$\rho_{xx}(T)$ [35]. However, the distinctive H and T dependence of ρ_{xx} (Figs. 6 and 9) suggests that $\zeta(T)$ at high H differs considerably from that at $H = 0$ (i.e., it is also a function of H), so that a different normalization strategy must be employed. Thus, the apparent discrepancy between the effective masses derived from SdH and dHvA effects is mainly attributable to $\zeta(H, T)$. Figure 7(a) shows a comparison for sample $N2$ of dHvA amplitudes and SdH amplitudes divided by ρ_{xx}^{BKG} at the same H. LK fits to the data for $T > 0.5$ K (i.e., where $\rho_{xx}^{\mathrm{BKG}} \propto T^{\alpha}$) yield cyclotron masses from dHvA and SdH effects that are consistent within experimental uncertainties. This, and the fact that both sets of oscillations have the same frequency, strongly suggests that the same band of coherent quasiparticles (with an effective mass approximately equal to $7m_0$) is responsible for both effects in YbB$_{12}$. Our recent pulsed-field studies reveal that these fermions also contribute quantum oscillations in the high-field KM state of YbB$_{12}$ [36], acquiring additional features such as Zeeman splitting and a field-dependent SdH frequency.

The consistency between $\tau^{\mathrm{osc}}(T)$ and $\rho_{xx}^{\mathrm{osc}}/\rho_{xx}^{\mathrm{BKG}}$ breaks down below 0.5 K [Fig. 7(a)], as the latter exhibits nonmonotonic behavior, which is likely to be an artefact. (Note that this nonmonotonic T dependence of the SdH amplitudes results entirely from the normalization to the background resistivity, since the raw data are free from such behavior; see Supplemental Material [93].) Moreover, the mass consistency is not as good for sample Ha, in which the ρ_{xx}^{osc} normalized to $\rho_{xx}^{\mathrm{BKG}} - \rho_{xx}^0$ [i.e., the T^{α} term in the inset of Fig. 6(b)] still gives a heavier mass $(m^*/m_0 = 9.4 \pm 0.7)$ than that from the dHvA effect $(m^*/m_0 = 6.4 \pm 0.1)$, as shown in Fig. 7(b). Nevertheless, the value of SdH mass becomes closer to the dHvA mass after the normalization; by contrast, the LK fit of the absolute SdH amplitudes provides $m^*/m_0 = 12.3 \pm 0.7$ [Fig. 7(b)]. Despite the additional complexity of the T-dependent background resistivity, the LK description is valid for the dHvA effect observed between 35 and 45 T [Figs. 7(a) and 7(b)] as well as the normalized SdH effect for 25.5 T $\leq \mu_0 H \leq 30$ T [Fig. 5(c)]. As the LK formula is closely related to the derivative of the Fermi-Dirac distribution function, this is an unambiguous sign that the quantum oscillations in both field ranges are produced by fermions.

VI. DISCUSSION

A. The two-fluid scenario

The transport properties of YbB$_{12}$ in its KI state point to the presence of both a Fermi surface of coherent quasiparticles (which, however, carry little or no charge) and electrically active charge carriers (some or all of which never gain full quasiparticle coherence) that are characteristic of a complex electrical insulator. This evidence may be summarized as follows.

Fermi surface of coherent quasiparticles:
(1) Quantum oscillations (both dHvA and SdH effects) are detected, with behaviors that are in agreement with the expectations for a 3D Fermi liquid.
(2) There is a cascade of signatures in the magnetic torque, Hall effect, and magnetoresistance strongly suggesting field-induced Lifshitz transitions that change the topology of the Fermi surface.
(3) A finite, residual T-linear thermal conductivity, a clear hallmark of itinerant gapless fermions, is observed as $T \to 0$ [39].
Complex electrical insulator:
(4) Both zero-field and high-field resistivities exhibit characteristic nonmetallic behavior; at high magnetic fields, this is described using a $T^{\alpha}(\alpha < 0)$ dependence.
(5) The absolute value of the resistivity is much larger than that of conventional metals [35].
(6) Apart from brief excursions due to the SdH oscillations, the underlying MR is negative for all fields up to the I-M transition.
(7) The Hall coefficient shows a low-field anomaly that cannot be explained by the conventional Drude model for metals. However, the form of the Hall coefficient is very similar to that of incoherent quasiparticles in the strange-metal phase regime of high-T_c superconductors.

In Ref. [36], we used a two-fluid model to give a phenomenological description of YbB$_{12}$ in both its KI and KM states. In the latter state, the fluids are (i) the conventional (heavy-fermion) charge carriers liberated by the collapse of the Kondo gap at high fields and (ii) a Fermi-surface of charge-neutral quasiparticles. In the KI state, (i) a complex system of charge-carrying electrons and holes containing both thermally activated carriers and other charged in-gap states (see Sec. VI B) coexists with (ii) the same charge-neutral quasiparticles. Under magnetic fields, the charge-neutral quasiparticles develop Landau levels that lead to an oscillatory DOS. In both KI and KM states, these oscillations in DOS result in the SdH effect in the resistivity due to strong scattering between the two fluids (at a rate that is determined by the joint DOS and hence the Landau quantization).

Taken alongside other recent experimental observations, the Hall-effect data in this paper permit a better description of the involved system of charge-carrying electrons and holes in the KI state than has previously been possible. We therefore first turn to the likely origin of these carriers.

B. Charge-carrying electrons and holes

The conventional explanation for mobile electrons and holes in a KI at low T is thermal excitation across the gap. The fact that the zero-field resistivity of YbB$_{12}$ can be fitted using an Arrhenius formula over the range $6 \lesssim T \lesssim 50$ K [35], albeit with two different gaps for lower- and

higher-temperature regimes, is good evidence that this mechanism does, in fact, contribute. However, below $T \approx 2$ K, the resistivity saturates, suggesting that as the number of thermally activated carriers declines as $T \to 0$, another mechanism starts to dominate.

Various origins have been proposed for the neutral quasiparticles in YbB$_{12}$, including 3D Majorana fermions (a consequence of the mixed-valence of Yb) [49,50], Majorana polarons [51], spinons [52,54], and related composite (fermionic) excitons [53], etc. The identity of the neutral fermions in YbB$_{12}$ is beyond the scope of the present work; however, we point out that all of the above approaches represent stationary states of an infinite, perfectly periodic crystal. The introduction of surfaces, grain boundaries, impurities, and other defects (and higher T) will result in the neutral fermion states possessing finite lifetimes. As the proposed neutral-quasiparticle models represent superpositions of electrons and holes, a likely decay or scattering route is into these charge-carrying in-gap states. An immediate consequence of such a mechanism is that the most perfect crystals of YbB$_{12}$ will show the *highest* values of saturated, low-T resistivity (i.e., the exact opposite of the situation in conventional metals). If one gauges crystal perfection using the absolute amplitudes of the KI-state SdH and dHvA oscillations (i.e., the larger the oscillations, the more perfect the crystal), this is indeed true for all of the samples we examine [35,39].

It is likely that when a neutral quasiparticle scatters off lattice defects or impurities, it will decay into an electron-hole pair. Such a process functions as indirect scattering between neutral and charged excitations; a change in the neutral-quasiparticle DOS will modify the scattering rate and thus be reflected in the number of charge carriers contributing to electrical transport. In addition, direct scattering between neutral and charged quasiparticles will occur, most likely via a Baber process. (Baber processes describe the interband scattering between multiple electron reservoirs with different masses [106].) The direct scattering rate should be proportional to the joint DOS of the bands involved. Consequently, both scattering mechanisms [107] will convert features in the field-dependent DOS of the neutral quasiparticles to signatures in the electrical transport measurements (including the Lifshitz transitions and SdH effect, as we discuss below). A more detailed description of the scattering mechanisms in the two-fluid model must await further theoretical work.

C. Temperature- and field-dependent Hall effect: Surface vs bulk conduction

Whereas several measurements [32,35,36,39] demonstrate that the neutral fermions and the thermally activated electrons and holes inhabit the bulk of YbB$_{12}$ (and are therefore definite intrinsic properties), studies of the focused-ion-beam (FIB)-etched YbB$_{12}$ samples reveal a substantial surface contribution at low T and low H [32]:

As H increases, charge transport in YbB$_{12}$ undergoes a crossover from surface dominated to bulk dominated, while the SdH effect arises only from bulk states.

Taking the above points into account, we assign the low-field Hall anomaly shown in Fig. 1 to the surface conduction channel, whereas the T-dependent Hall signal at higher fields is associated with the bulk. Consequently, the analysis in Sec. III points to the incoherent nature of the extended surface states in YbB$_{12}$: Their behavior is analogous to that of the strange-metal phase in correlated-electron systems [56–58]. It is likely that several factors contribute to the loss of quasiparticle coherence at the surface: (i) There will be scattering of the surface charge carriers into the DOS associated with the charged fermions in the bulk of the material (similar surface-bulk scattering processes have been widely reported in candidate topological insulators [109,110] and Weyl semimetals [111]). (ii) In order to maintain neutral-fermion density, charged fermions at the surface will be subsumed into the bulk itinerant neutral states (the reverse of the process that creates them). (iii) There is also expected to be scattering due to magnetic fluctuations [76], which can be enhanced significantly at the surface where the Kondo interaction is weakened compared to the bulk [78,112].

We argue that the abundance of scattering process (iii), implicit in the Hall expression Eq. (1) and resembling those in quantum critical metals, is a major ingredient in the absence of SdH oscillations in the FIB microstructures [32]. Although the conducting surface states can also experience scattering with charge-neutral quasiparticles, strong scattering from the magnetic fluctuations at the surface may be the dominant process and perhaps cause a strange-metallic state at the surface. As a result, the neutral-quasiparticle DOS has only a small effect on the surface conduction, so that the SdH effect is suppressed below our experimental resolution. Other factors, such as the destruction of neutral-quasiparticle bands by Kondo breakdown at the surface [50,112], or the excess surface defects introduced by the FIB etching, may also contribute to a reduced neutral-quasiparticle lifetime, thus suppressing SdH oscillations.

D. Putative Lifshitz transitions

As increasing magnetic field suppresses the Kondo gap [61], the bulk transport channels come into play. The first characteristic field manifested by the upturn in τ and a cusp in the MR [35] occurs at $\mu_0 H_1 = 19.6$ T. Given that the ground state of Yb^{3+} in YbB$_{12}$ has Γ_8 symmetry with $g_J m_J = 2.1$ (here, g_J is the Landé g factor, and m_J is the magnetic quantum number for angular momentum) [62], the Zeeman energy E_z of the Γ_8 multiplets at $H = H_1$ is 2.39 meV $\approx \Delta_2/2$, where $\Delta_2 = 4.70$ meV is the low-temperature transport gap determined from $\rho_{xx}(T)$ [35]. The close correspondence of these energies suggests that H_1 may be related to the Zeeman splitting of the crystal-electric-field (CEF) multiplets of the Yb f states. However,

H_1 is not a real gap-closing (i.e., I-M transition) field because there is no evidence for a sudden DOS enhancement at this field in transport data [35] and heat capacity [82] measurements (consequently, Δ_2 might be the energy separation between an in-gap impurity level and one of the band edges). The Hall coefficient data merely show a downward kink at H_1, suggestive of an inflection in DOS (H) [69]. These features are consistent with a Lifshitz transition, presumably in the FS of the charge-neutral fermions, that is related to the Zeeman shift of the CEF levels. Though we are not able to assign H_2 to possible CEF-level splitting effects, the distinct SdH frequencies detected below and above this field strongly imply that it can be another putative Lifshitz transition. At these transitions, the signatures in electrical transport may originate from abrupt changes of the interband scattering rate (which depends on the DOS of the neutral fermions) at the Lifshitz transitions.

Further studies of the field-dependent gap evolution in YbB$_{12}$ will provide insights into the nature of the characteristic fields H_1 and H_2; at this point, we propose that the Zeeman shift of the CEF levels causes the gap narrowing under magnetic fields, which modifies the dispersion of the in-gap neutral-quasiparticle bands and/or drives a relative energy shift between these bands and the chemical potential. Successive (putative) Lifshitz transitions can happen during this process before the complete closing of the charge gap. We mention that while field-induced CEF-level mixing can also lead to abrupt FS reconstructions [113], such effect remains very weak in YbB$_{12}$ up to $\gtrsim$40 T [114] and thus is likely to be irrelevant here (see Supplemental Material [93] for more information).

E. Mechanism for the quantum oscillations

The most important question in our study of YbB$_{12}$ is the origin of the quantum oscillations in the KI state. In our two-fluid picture (Fig. 8), this is attributed to Landau quantization of the charge-neutral FS and the interband scattering between charged- and neutral-fermion states [36]. In the present paper, our observation of the T^α dependence ($-2 \lesssim \alpha \lesssim -1.5$) of high-field ρ_{xx} data further supports this explanation by confirming that the charge carriers are not in a coherent FL state and therefore cannot cause the observed quantum oscillations. Instead, the neutral-fermion Landau levels modulate the scattering rate (Fig. 8) via the processes introduced in Sec. VI B, leading to the SdH effect in ρ_{xx}.

We again emphasize that, although the T dependence of the SdH amplitudes remains complex due to the plethora of scattering processes, the excellent fit of the dHvA amplitudes to the LK formula [Fig. 7(a), see also Refs. [35,36]] is a definitive signature of FL-like behavior. This explicitly supports the gapless neutral-fermion interpretation and
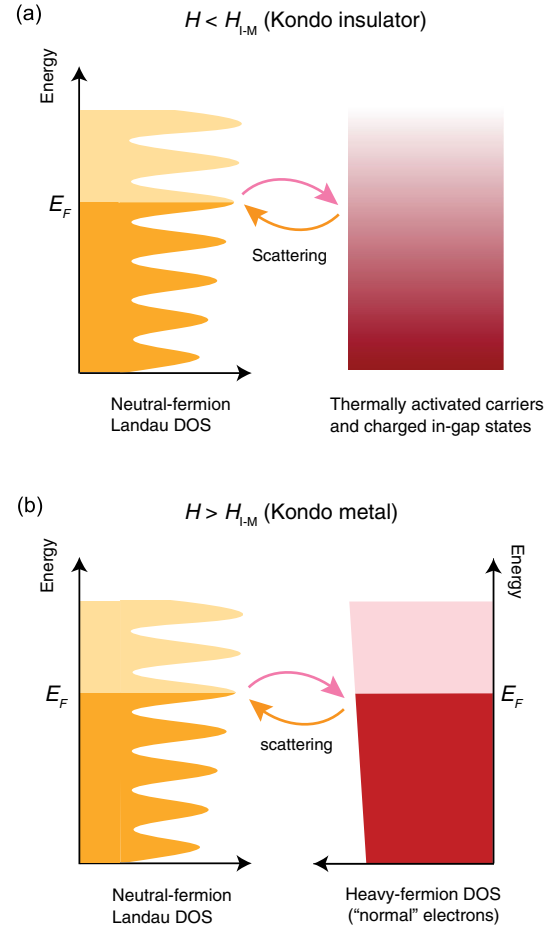

FIG. 8. Schematic of the two-fluid picture for transport in YbB$_{12}$; a neutral-quasiparticle Fermi surface coexists with more conventional charge carriers. Close to E_F, the neutral quasiparticles may likely be represented as a linear, equal combination of canonical particle and antiparticle operators. The linear coupling to the magnetic vector potential $\mathbf{A}$ will change their wave-vector ($\mathbf{k}$) dependent energy to $E = \frac{1}{2}\{\varepsilon[\mathbf{k} - (e/\hbar)\mathbf{A}] + \varepsilon[\mathbf{k} + (e/\hbar)\mathbf{A}]\}$. Thus, any linear response to $\mathbf{A}$ (e.g., electrical conductivity) will be zero, but effects quadratic in $\mathbf{A}$ (e.g., Landau quantization, and therefore, the dHvA effect) will occur. (a) In the KI state, the charge carriers are primarily thermally activated electrons and holes plus (for $T \lesssim 2$ K) charged in-gap states including surface states, bulk impurity levels, etc. The rate of scattering between the charge carriers and the neutral quasiparticles will depend on the available DOS; hence, the Landau-level DOS of the neutral quasiparticles will cause a field-dependent modulation of the electrical transport, leading to SdH oscillations. (b) In the KM state, fermions scatter between charge-neutral Landau levels and heavy-fermion metal bands; again, the scattering occurs at a rate given by the joint fermion DOS. As the neutral-quasiparticle DOS oscillates with H, so will the transport parameters of the heavy electrons. [The heavy electrons are thought to have a mass approximately equal to $100m_0$, and so their quantum oscillations will be thermally smeared out even at the lowest experimental T thus far [36].]

indeed helps us to rule out most of the alternative scenarios. Numerous hypothetical models predict that quantum oscillations can emerge in *gapped* electronic systems through the field-induced tunneling effect [115,116], exciton formation [117], periodic variation of the gap width [118–122] or Kondo-coupling strength [123], or Landau quantization of band-edge states in conjunction with a sharp slope change in a fully filled band [124]. All of these *gapped* models cannot explain the experimental T dependence of the quantum oscillations in YbB$_{12}$ because they predict non-LK behavior of the oscillation amplitudes or even a complete absence of the SdH effect.

Another question is whether or not a disorder-induced nodal semimetal phase could contribute to or cause the quantum oscillations [99,100]. In such a phase, the (incoherent) non-Hermitian in-gap states, despite being characterized by a finite quasiparticle lifetime, can form Landau levels under magnetic fields and produce quantum oscillations with LK-like behavior [99]. At present, we cannot completely rule out this possibility, since the T^{α} dependence of ρ_{xx} may also suggest nodal transport, as discussed in Sec. V B. However, this scenario is unlikely because of its prediction of an apparent mass term in the LK expression that is determined by the scattering rate [99]. Immediately above H_{I-M}, the boosted population of charged fermions [82] should change the scattering rate significantly, yet the mass obtained from LK fits is still very close to that below H_{I-M} (approximately equal to $7m_0$) [36]. This strongly suggests that the scattering rate does not affect the measured effective mass. Hence, we believe that the incoherent charge carriers in the KI state of YbB$_{12}$ are incapable of developing Landau quantization themselves, and the SdH effect comes from their scattering with the Landau-quantized neutral fermions (see Fig. 8).

We also note that quantum oscillations in the resistivity and magnetization of YbB$_{12}$ have been observed by a Cambridge group [37,125]. Some of the orbit areas and cyclotron masses that they reported are similar to our results. The Cambridge group further mentions that, unlike SmB$_6$ in which the quantum-oscillation patterns match the large FSs in the absence of hybridization [34,38], the quantum oscillations in YbB$_{12}$ stem from small FS pockets of neutral quasiparticles. Despite these consistencies, their samples show remarkably low resistivity for a KI: The low-$T\rho_{xx}$ of only approximately 0.01 Ω cm [37], 2 order of magnitudes smaller than that of our samples, is likely attributable to a higher concentration of impurities (see discussion above and Ref. [45]). Therefore, owing to the sensitivity of the Kondo gap and the various low-energy scattering effects to impurities [126–129], the phenomena observed in the two types of YbB$_{12}$ sample, while being part of the same unified picture, may differ substantially.

VII. CONCLUSIONS

In summary, we report a detailed study of electrical transport and magnetic torque in the KI YbB$_{12}$ under the extreme conditions of low temperatures and high magnetic fields. A low-field Hall anomaly with an unusual nonlinear-H profile is revealed for $T \lesssim 1.5$ K; this cannot be explained by a standard two-band Drude model and is instead assigned to the contribution from strange-metal-like non-FL states (most likely residing on the surfaces) without full quasiparticle coherence. At $\mu_0 H_1 = 19.6$ T, a prominent signature appears in both MR and τ, coinciding with a slope change in the Hall coefficient. A similar, but less prominent, signature is observed at $\simeq 30.4$–31.3 T with a weak sample dependence. We interpret these as putative field-induced Lifshitz transitions that, in a similar manner to the SdH oscillations in YbB$_{12}$, occur in the FS of exotic charge-neutral fermions and are manifested in transport via scattering with the charge carriers (Fig. 8). We further show that the apparent different T dependences of the dHvA and the SdH oscillation amplitudes are mainly caused by a T^{α} behavior of the background resistivity, with α being H dependent ($-2 \lesssim \alpha \lesssim -1.5$). This suggests the high-field charge transport in YbB$_{12}$ is subject to unusual scattering mechanisms that are very different from those in normal metals.

The above results strongly support a two-fluid model involving of two type of fermions: one set behaving like a conventional FL, yet not carrying charge; the other comprising charge carriers that exhibit incoherent, non-FL-like electrical transport. The interplay between the two fluids gives rise to the unusual transport phenomena including the possible Lifshitz transitions and the SdH effect (in a KI state). While our study provides solid evidence for the presence of charge-neutral quasiparticles in YbB$_{12}$, further investigation is under way to clarify their exact nature.

APPENDIX A: LOW-TEMPERATURE RESISTIVITY

The longitudinal resistivity ρ_{xx} in sample $N2$ is displayed in Fig. 9 for $T < 1.3$ K. ρ_{xx} increases slowly with cooling down, and appears to saturate for $T \lesssim 0.2$ K. Note that the T range shown in Fig. 9 is within the "resistive plateau" [35] in YbB$_{12}$ which occurs below $T \approx 2.2$ K. The T dependence of ρ_{xx} between 0.25 and 1 K can be fitted by a simple function that invokes both surface and bulk transport channels:

$$\rho_{xx}(T) = \frac{1}{G_s/t + \sigma_b} = \frac{1}{G_s/t + \xi_N T}, \qquad \text{(A1)}$$

where G_s is the surface conductance, t is the sample thickness, and $\sigma_b = \xi_N T$ is the bulk conductivity which is linear in T.

The fit (red line in Fig. 9) yields $G_s = 4.05 \times 10^{-3}\ \Omega^{-1}$ (corresponding to a surface resistance of 246.9 Ω) and $\xi_N = 0.0314\ \Omega^{-1}\,\text{cm}^{-1}\,\text{K}^{-1}$. We note that Eq. (A1) decomposes the overall resistivity into two contributions: one from a T-independent surface conduction, the other due to a bulk conduction which varies linearly with T. The same formula has been proposed to interpret the low-T resistive plateau in SmB$_6$ [100], where the T-linear bulk conductivity is taken as evidence for the formation of gap nodes due to the impurity-scattering-induced level broadening. Following the analysis in Ref. [100], the node conductivity is given as
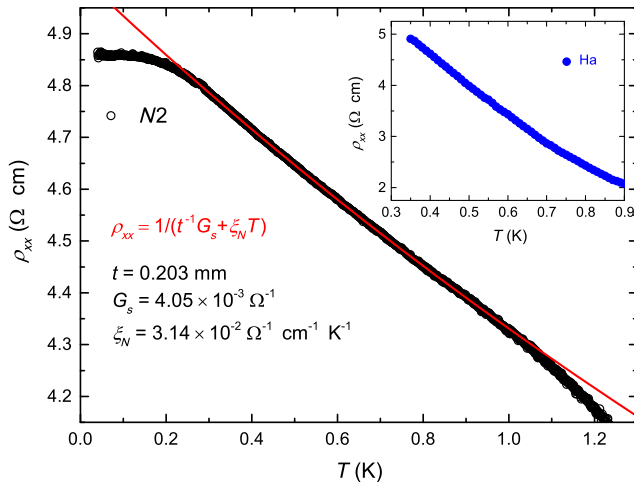

FIG. 9.   Resistivity ρ_{xx} of sample $N2$ as a function of the temperature below $T = 1.3$ K measured in a dilution refrigerator. Between 0.3 and 1.0 K, ρ_{xx} of sample $N2$ can be fitted by $\rho_{xx} = (G_s/t + \xi_N T)^{-1}$ (see text) (solid line). The fitting parameters are also shown. The inset shows the low-temperature resistivity of YbB$_{12}$ sample Ha.

$$\xi_N = \frac{\ln 2}{4\pi^3} \frac{k_B e^2 S_k}{\hbar k_0} \frac{\Gamma_0}{V^2}. \qquad \text{(A2)}$$

Here, S_k is the Fermi-surface area for the unhybridized conduction band, k_0 represents the position of the impurity-induced nodes in momentum space, whereas Γ_0 and V are the energy-level broadening and the hybridization potential, respectively. By using the electrical-transport results ($\Delta_2 = 3.2$–4.7 meV), quantum-oscillation data ($F \approx 700$ T, $m^*/m_0 \approx 7$) [35,36], and ARPES results [33] in YbB$_{12}$, we estimate $k_0 \approx 0.2$ Å^{-1} and $V \simeq 9.2$–11.5 meV. Therefore, the fitted $\xi_N = 0.0314\ \Omega^{-1}\,\text{cm}^{-1}\,\text{K}^{-1}$ corresponds to $\Gamma_0 S_k \approx 7$–11×10^{-4} Jm^{-2}. To close the hybridization gap at k_0 by node formation, the level broadening needs to be $\Gamma_0 \geq 2V \approx 20$ meV. If the system is actually driven into a nodel semimetal phase by impurity scattering, the value of S_k would be only 0.2–0.3 nm^{-2} (corresponding Fermi vector $k_F \lesssim 0.3$ nm^{-1}). Such a small Fermi surface area obviously contradicts that observed in our quantum-oscillation measurements ($k_F \simeq 1.4$–1.7 nm^{-1}) [35] and is even more inconsistent with the calculated large-d-electron pockets for unhybridized YbB$_{12}$ [37]. We thus conclude that the behavior of $\rho_{xx}(T)$ in YbB$_{12}$ cannot be explained by the impurity-induced nodal in-gap states.

Moreover, our recent transport study of FIB-etched YbB$_{12}$ microstructures also confirms the validity of Eq. (A1) in describing the low-T resistivity. However, in that case, the term ξ_N was revealed to be thickness dependent [32]. This provides further evidence that the T-linear term is not solely associated with the bulk states. We also mention that the low-T ρ_{xx} shows different behavior between batches. As displayed in the inset of Fig. 8, ρ_{xx} in sample Ha exhibits a stronger T dependence compared to sample $N2$ below 1 K. $\rho_{xx}(T)$ of sample Ha cannot be successfully fitted by Eq. (A1). These differences presumably reflect the different surface conditions on the various samples, since the low-temperature, low-field electrical transport in YbB$_{12}$ seems to be dominated by surface contributions [32].

We mention that our experimental results for YbB$_{12}$ microstructures [32] cannot completely rule out the existence of bulk conducting channels at zero temperature. A recent theoretical work predicts that a low-T resistivity, saturation can originate from bulk states in a "quantum-conduction" regime beyond the conventional Boltzmann picture [130]. Such a scenario, however, is to be tested for YbB$_{12}$ only after the dominating surface conduction at low T (as confirmed by the highly thickness-dependent resistivity below the saturation [32]) can be isolated using unique measurement configurations, e.g., the double-sided Corbino device [131]. We emphasize that the presence of a small residual bulk conduction will not invalidate the main conclusions of this work.

APPENDIX B: MAGNETORESISTANCE

Charge transport in the ground state of YbB_{12} is characterized by a negative MR, which reaches -37% at $\mu_0 H = 18$ T ([Fig. 10(a)]. This negative MR was previously believed to stem from the field suppression of the Kondo gap through the Zeeman splitting of the f-electron multiplets [61,62]. Recently, we demonstrated that for $T < 1$ K, the MR in the low-H region (up to 8 T) can be accounted for by the Hikami-Larkin-Nagaoka model for weak antilocalization, while the gap suppression explanation works for the negative MR at higher fields [32]. Nevertheless, the negative MR corroborates that the electrical-transport properties of YbB_{12} cannot be described by the classical two-band model that predicts an enhanced positive orbital contribution to the MR [132].

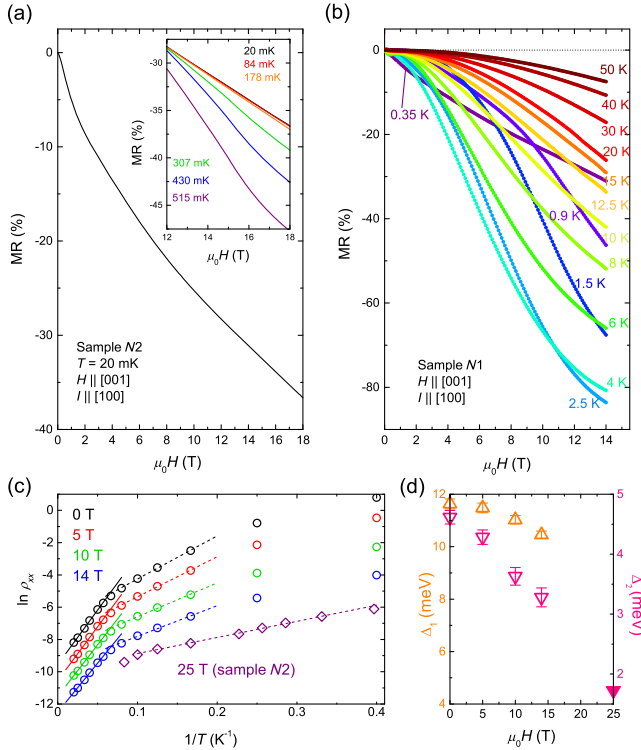FIG. 10.   (a) Transverse MR $[\rho_{xx}(H)\text{-}\rho_{xx}(0)]/\rho_{xx}(0) \times 100\%$ measured in sample $N2$ at $T = 20$ mK, with magnetic field up to 18 T applied along [001] and current $I\parallel$ [100]. Inset exhibits transverse MR of sample $N2$ between 12 and 18 T at various temperatures. (b) Transverse MR of sample $N1$ up to 14 T for temperatures between 0.35 and 50 K. (c) The Arrhenius plot $\ln\rho_{xx}$ versus $1/T$ for sample $N1$ under different magnetic fields up to 14 T (hollow circles). The slopes of the linear fits for temperature ranges 17.5 K $\leq T \leq 50$ K (solid lines) and 6 K $\leq T \leq 12.5$ K (dashed lines) give the value of gap widths Δ_1 (up triangles) and Δ_2 (down triangles) in (d), respectively. Data taken in sample $N2$ at 25 T are also displayed with the linear fit between 3 and 8 K yielding $\Delta_2 = 1.725$ meV [solid down triangle in (d)]. The plots are shifted vertically by 1 for clarity.

As shown in the inset of Figs. 10(a) and 10(b), the negative transverse MR (measured with $H \perp I$) in YbB_{12} first increases upon warming, reaches a maximum of -83.5% at 14 T and $T = 2.5$ K, then gradually decreases as T increases further. No positive MR is observed up to 50 K. We conclude that the low-T charge transport in YbB_{12} exhibits distinct nonmetallic behavior and thus cannot be explained within the frame of 3D bandlike quasiparticle transport theory. Figure 10(c) displays Arrhenius plots $\ln\rho_{xx}$ versus $1/T$ for different magnetic fields. As noted previously [35], two gap widths (Δ_1 and Δ_2) can be obtained from the linear fits within the temperature ranges 17.5 K $\leq T \leq 50$ K and 6 K $\leq T \leq 12.5$ K, respectively. The field dependence of the two gap widths is shown in Fig. 10(d). It appears that the low-temperature transport gap Δ_2 is more severely affected by magnetic field, decreasing by roughly one third at 14 T compared to the approximately 10% suppression for Δ_1. This phenomenon is consistent with earlier reports in both YbB_{12} [61] and SmB_6 [30].

At 25 T, the linear fit does not work in the same temperature window for Δ_2, yet the slope between 3 and 8 K gives a gap width of 1.725 meV, i.e., less than 40% of the zero-field value [Fig. 10(c)]. We add this point to Fig. 10(d) as a solid triangle. With H further increasing, however, the linear section in $\ln\rho_{xx}$ versus T^{-1} cannot be determined, and ρ_{xx} develops the T^{α} ($\alpha < 0$) behavior seen above 35 T (Fig. 6).

APPENDIX C: TWO-BAND ANALYSIS OF THE HALL COEFFICIENT

In most cases, a nonlinear $\rho_{xy}(H)$ is taken as evidence for a multiband carrier system comprising electrons and holes. Here, we define a field-dependent Hall coefficient $R_H \equiv \rho_{xy}/\mu_0 H$ and plot it as a function of H for $T = 20$ mK in Fig. 1(b). For $H \rightarrow 0$, R_H is negative; as H ramps up, R_H is quickly suppressed, crossing zero at approximately 6.6T. It then shows a very weak downward bending for $\mu_0 H > 10$ T. We first focus on the low-H region below 10 T where the field dependence of R_H is most evident. Standard Boltzmann-transport theory provides an expression for R_H in a two-band system [72,133]:

$$R_H(H) = \frac{1}{e} \frac{(n_h\mu_h^2 + n_e\mu_e^2) + (n_h - n_e)\mu_h^2\mu_e^2(\mu_0 H)^2}{(n_h\mu_h + n_e\mu_e)^2 + (n_h - n_e)^2\mu_h^2\mu_e^2(\mu_0 H)^2}, \tag{A3}$$

where n_h is the density of holes, n_e the density of electrons, μ_h the hole mobility, and μ_e the electron mobility. We apply Eq. (A3) to the $R_H(H)$ values shown in Fig. 1(b) with the parameters n_h, n_e, μ_h, and μ_e further constrained using the value of the zero-temperature resistivity $\rho_{xx}(0) = (en_h\mu_h + en_e\mu_e)^{-1} = 4.85$ $\Omega\,\text{cm}$ (Fig. 9). Following the discussion in Ref. [134], we can write R_H as
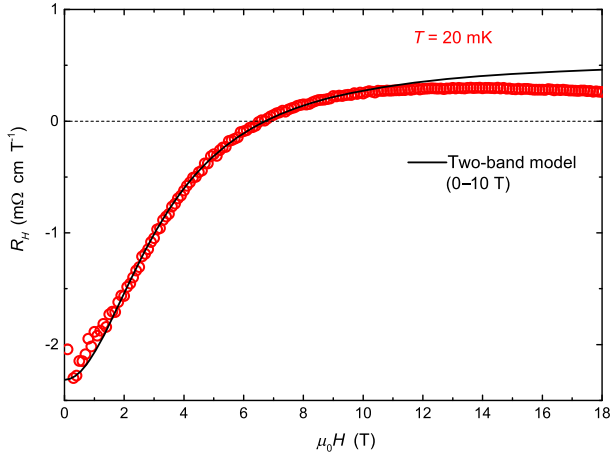
FIG. 11. Fitting of the field dependence of the Hall coefficient $R_H(H)$ below 10 T using a two-band model with the constraint from the zero-field resistivity [Eq. (A4) in Appendix C]. $R_H(H)$ is measured in sample N2 at $T = 20$ mK.

$$R_H = \rho_{xx}(0) \frac{a + b(\mu_0 H)^2}{1 + c(\mu_0 H)^2}, \qquad (A4)$$

where $a = f_h \mu_h - f_e \mu_e$, $b = -(f_e \mu_h - f_h \mu_e)\mu_h \mu_e$, $c = (f_h \mu_e - f_e \mu_h)^2$, and $f_{h,e} = (n_{h,e}\mu_{h,e})/(n_h \mu_h + n_e \mu_e)$. Hence, the number of fitting parameters is reduced to three: μ_h, μ_e, and f_h ($f_e = 1 - f_h$). The fitting curve using Eq. (A4) is displayed in Fig. 11. From this fit, we obtain the following parameters: $n_h = (1.13 \pm 0.01) \times 10^{18}$ cm^{-3}, $n_e = (8.20 \pm 0.05) \times 10^{11}$ cm^{-3}, $\mu_h = 1.1 \pm 0.1$ cm^2 V^{-1} s^{-1}, and $\mu_e = 3045 \pm 32$ cm^2 V^{-1} s^{-1}. Notably, the fitting parameters point toward the existence of a very small electron pocket with relatively high mobility. Taking into account possible surface conduction, we can assume that the electron pocket, which has a lower carrier density, is associated with 2D surface states, while the holes inhabit the bulk of the sample. However, the fitted n_e converts to a 2D carrier density $n_e^{2D} = (1.66 \pm 0.02) \times 10^{10}$ cm^{-2} which is 3 orders of magnitude lower than $n_e^{2D} = 5.16 \times 10^{13}$ cm^{-2} determined from the ARPES results [33] [$k_F \simeq 0.18$ Å^{-1} for the surface state on the (001) surface; the possible lifting of spin degeneracy is not considered here]. Indeed, the small n_e^{2D} yielded by the two-band fit corresponds to $k_F = 0.0323$ nm^{-1} and a quantum-oscillation frequency $F = 0.343$ T under the assumption of an isotropic FS. While we cannot completely exclude the existence of such tiny surface FS pockets, no further supporting evidence for them has been revealed by ARPES [33] and transport [32,35]. Additionally, the two-band model [Eq. (A4)] does not give a perfect fit for the evolution of R_H from 2 T to approximately 5 T [i.e., around the maximum of $\rho_{xy}(H)$]. It also fails to track the behavior of R_H above 10 T.

We further mention that it is impossible to perform simultaneous fits to $\rho_{xy}(H)$ and $\rho_{xx}(H)$ [58,135] in YbB$_{12}$: Whereas the two-band Drude model predicts a positive MR due to the orbital motion of carriers in magnetic field, in YbB$_{12}$ the MR is always negative (Appendix B). The absence of positive MR indeed strongly challenges the validity of the two-band Drude description. The nonmetallic $\rho_{xx}(T)$ (Appendix A) also clearly deviates from Drude-like behavior. Moreover, aside from the single-surface FS pocket detected by ARPES [33], there is no experimental evidence for the existence of FSs of charge carriers in YbB$_{12}$. Therefore, despite the two-band models failing to yield satisfactory fits, there is no reason to add a third band to improve the fit quality. Taking all of these factors into account, the low-field Hall anomaly in YbB$_{12}$ characterized by an usual H-nonlinear behavior cannot be attributed to multiband effects.

APPENDIX D: IDENTIFICATION OF THE CHARACTERISTIC FIELDS

Multiple-field-induced signatures appear in different physical quantities of YbB$_{12}$ below H_{I-M} (Fig. 4). Identification of these signatures should be assigned with caution, because quantum oscillations occurring in different field ranges (Fig. 5) can manifest as features resembling field-induced transitions. In Fig. 12(a), we plot MR and $d\tau/dH$ of sample Ha together to provide insights into the nature of these signatures. Most remarkably, the features (two valleys and one peak) appearing between 25.5 and 30.5 T [yellow shaded region in Fig. 12(a)] are well aligned between the two quantities $d\tau/dH$ and ρ_{xx}, exactly as what is expected for quantum oscillations [92]. Hence, we identify the signature at 28 T (arrows in Figs. 4 and 12) to be a quantum-oscillation extremum, i.e., the SdH peak shown in Fig. 5(b). The consistency of the location of this feature between the up-sweep and down-sweep MR curves [vertical dashed line in Fig. 12(a)] further supports this assignment.

We identify the kink [crossing of the two black straight lines in Fig. 12(a)] in $d\tau/dH$ as another putative Lifshitz transition H_2 in addition to H_1. The slightly different locations of this signature [$\simeq$30.4 T in Fig. 4(b) and 30.6 T in Fig. 12(a)] are likely due to a small change in field orientations. This transition is probably the one leading to the SdH frequency change as shown in Fig. 5. We note that the position of H_2 may have a displacement for the MR up sweeps and down sweeps [Fig. 4(c)], yet such a displacement is missing for magnetic torque data [Fig. 12(a)]. Since torque and MR are measured in static and pulsed magnetic fields, respectively, the displacement may be related to mechanisms with slow kinetics that have relaxation rates similar to the rate of change of the pulsed fields. Indeed, mismatches between the up sweeps and
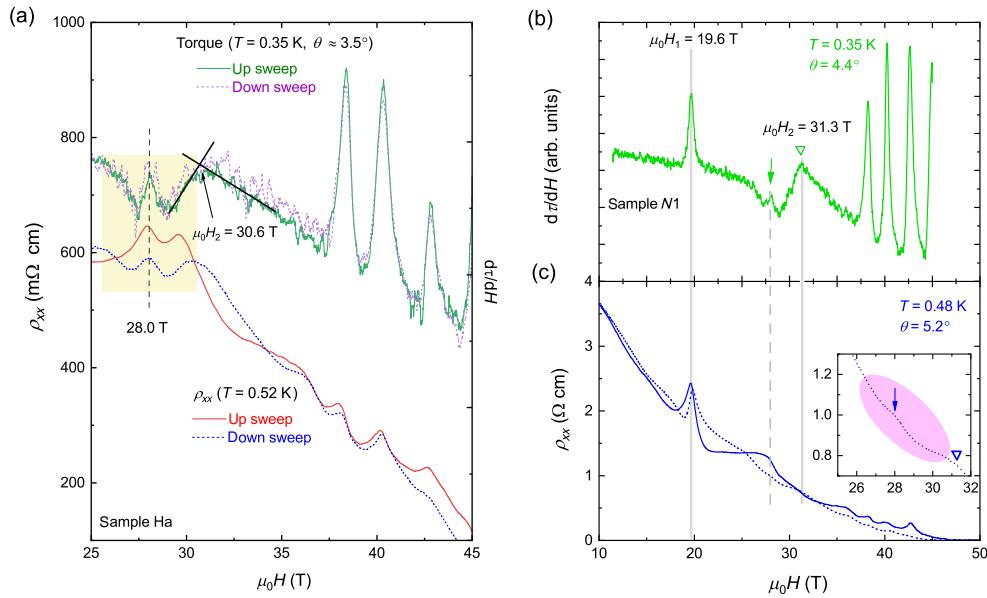
FIG. 12.   (a) Magnetic field dependence of MR and $d\tau/dH$ for the YbB$_{12}$ sample Ha, with the magnetic field close to the [001] direction. Solid and short-dashed lines represent data curves taken during field up sweep and down sweep, respectively. To be noted, two wiggles appear between 25.5 and 30.5 T (yellow shaded region) with the peaks and valleys well aligned between ρ_{xx} and $d\tau/dH$. These are quantum oscillations. In particular, the signature at 28 T (vertical dashed line) should be a SdH peak. An abrupt slope change of $d\tau/dH$ at 30.6 T, on the other hand, is likely to be a Lifshitz transition. Magnetic field dependence of (b) $d\tau/dH$ measured at $T = 0.35$ K for tilt angle $\theta = 4.4°$, (c) MR at $T = 0.48$ K for $\theta = 5.2°$. Data in (b) and (c) are measured in sample $N1$. Solid and short-dashed lines in (c) are up sweeps and down sweeps, respectively. Characteristic fields $\mu_0H_1 = 19.6$ T (manifested by prominent peaks in both $d\tau/dH$ and MR) and $\mu_0H_2 = 31.3$ T (a sharp kink in $d\tau/dH$) are denoted by vertical solid gray lines. The feature appearing at 28 T in both $d\tau/dH$ and MR (arrow and dashed vertical line) originates from quantum oscillations. Inset of (c) is an expanded view of $\rho_{xx}(H)$ between 25 and 32 T. The light magenta shaded area indicates the field range at which hints of a weak SdH effect can be seen on the down sweep. The down triangle marks the position of μ_0H_2.

down sweeps in the MR measurement are more pronounced in the vicinity of the characteristic fields H_1 and H_2; this might suggest a first-order-like nature of the Lifshitz transitions that has been proposed for systems with substantial electron correlations [136].

In Figs. 12(b) and 12(c), we display the field dependence of $d\tau/dH$ and ρ_{xx} of sample $N1$, respectively. Two sharp anomalies in $d\tau/dH$ are identified as the characteristic fields H_1 (gray vertical line) and H_2 (down triangle), whereas an additional signature at 28 T represents a quantum-oscillation maximum in both ρ_{xx} and $d\tau/dH$ (arrows and the vertical dashed line). There are several points to be mentioned. The position of H_1 is consistent with that in sample Ha; i.e., this signature shows no sample dependence. On the other hand, the characteristic field H_2 associated with the sharp kink in $d\tau/dH$ [Fig. 12(b)] is much less evident in sample Ha [Figs. 4(b) and 12(a)]; its position varies slightly between samples ($\mu_0H_2 = 30.4 \pm 0.2$ T and 31.3 T for sample Ha and $N1$, respectively). The SdH oscillations between 25.5 and 30 T [the shaded area in the inset of Fig. 12(b)] are much weaker than those in sample Ha [Fig. 4(c)]; this is why they were overlooked in our previous work [35].

[1] A. C. Hewson, *The Kondo Problem to Heavy Fermions* (Cambridge University Press, Cambridge, England, 1993).

[2] P. S. Riseborough, *Heavy Fermion Semiconductors*, Adv. Phys. **49**, 257 (2000).

[3] P. Coleman, in *Many-Body Physics: From Kondo to Hubbard*, edited by E. Pavarini, E. Koch, and P. Coleman (Forschungszentrum, Jülich, 2015).

[4] C. M. Varma, *Aspects of Strongly Correlated Insulators*, Phys. Rev. B **50**, 9952 (1994).

[5] A. Menth, E. Buehler, and T. H. Geballe, *Magnetic and Semiconducting Properties of* SmB$_6$, Phys. Rev. Lett. **22**, 295 (1969).

[6] M. Kasaya, F. Iga, M. Takigawa, and T. Kasuya, *Mixed Valence Properties of* YbB$_{12}$, J. Magn. Magn. Mater. **47–48**, 429 (1985).

[7] M. F. Hundley, P. C. Canfield, J. D. Thompson, Z. Fisk, and J. M. Lawrence, *Hybridization Gap in* Ce$_3$Bi$_4$Pt$_3$, Phys. Rev. B **42**, 6842 (1990).

[8] T. Caldwell, A. P. Reyes, W. G. Moulton, P. L. Kuhns, M. J. R. Hoch, P. Schlottmann, and Z. Fisk, *High-Field Suppression of In-Gap States in the Kondo Insulator* SmB$_6$, Phys. Rev. B **75**, 075106 (2007).

[9] M. Okawa, Y. Ishida, M. Takahashi, T. Shimada, F. Iga, T. Takabatake, T. Saitoh, and S. Shin, *Hybridization Gap Formation in the Kondo Insulator* YbB$_{12}$ *Observed Using Time-Resolved Photoemission Spectroscopy*, Phys. Rev. B **92**, 161108(R) (2015).

[10] J. C. Cooley, M. C. Aronson, Z. Fisk, and P. C. Canfield, SmB₆Lo *Kondo Insulator or Exotic Metal?*, Phys. Rev. Lett. **74**, 1629 (1995).

[11] M. Dzero, K. Sun, V. Galitski, and P. Coleman, *Topological Kondo Insulators*, Phys. Rev. Lett. **104**, 106408 (2010).

[12] M. Dzero, K. Sun, P. Coleman, and V. Galitski, *Theory of Topological Kondo Insulators*, Phys. Rev. B **85**, 045130 (2012).

[13] V. Alexandrov, M. Dzero, and P. Coleman, *Cubic Topological Kondo Insulators*, Phys. Rev. Lett. **111**, 226403 (2013).

[14] T. Takimoto, SmB₆*: A Promising Candidate for a Topological Insulator*, J. Phys. Soc. Jpn. **80**, 123710 (2011).

[15] F. Lu, J. Z. Zhao, H. Weng, Z. Fang, and X. Dai, *Correlated Topological Insulators with Mixed Valence*, Phys. Rev. Lett. **110**, 096401 (2013).

[16] M. Neupane, N. Alidoust, S.-Y. Xu, T. Kondo, Y. Ishida, D. J. Kim, C. Liu, I. Belopolski, Y. J. Jo, T.-R. Chang, H.-T. Jeng, T. Durakiewicz, L. Balicas, H. Lin, A. Bansil, S. Shin, Z. Fisk, and M. Z. Hasan, *Surface Electronic Structure of the Topological Kondo-Insulator Candidate Correlated Electron System* SmB₆, Nat. Commun. **4**, 2991 (2013).

[17] J. Jiang, S. Li, T. Zhang, Z. Sun, F. Chen, Z. R. Ye, M. Xu, Q. Q. Ge, S. Y. Tan, X. H. Niu, M. Xia, B. P. Xie, Y. F. Li, X. H. Chen, H. H. Wen, and D. L. Feng, *Observation of Possible Topological In-Gap Surface States in the Kondo Insulator* SmB₆ *by Photoemission*, Nat. Commun. **4**, 3010 (2013).

[18] N. Xu *et al.*, *Direct Observation of the Spin Texture in* SmB₆ *as Evidence of the Topological Kondo Insulator*, Nat. Commun. **5**, 4566 (2014).

[19] Y. Ohtsubo, Y. Yamashita, K. Hagiwara, S. Ideta, K. Tanaka, R. Yukawa, K. Horiba, H. Kumigashira, K. Miyamoto, T. Okuda, W. Hirano, F. Iga, and S. Kimura, *Non-Trivial Surface States of Samarium Hexaboride at the (111) Surface*, Nat. Commun. **10**, 2298 (2019).

[20] D.-C. Ryu, C.-J. Kang, J. Kim, K. Kim, G. Kotliar, J.-S. Kang, J. D. Denlinger, and B. I. Min, *Topological Surface States on the Nonpolar (110) and (111) Surfaces of* SmB₆, Phys. Rev. B **103**, 125101 (2021).

[21] L. Miao, C.-H. Min, Y. Xu, Z. Huang, E. C. Kotta, R. Basak, M. S. Song, B. Y. Kang, B. K. Cho, K. Kißner. F. Reinert, T. Yilmaz, E. Vescovo, Y.-D. Chuang, W. Wu, J. D. Denlinger, and L. A. Wray, *Robust Surface States and Coherence Phenomena in Magnetically Alloyed* SmB₆, Phys. Rev. Lett. **126**, 136401 (2021).

[22] L. Jiao and S. Rößler, D. J. Kim, L. H. Tjeng, Z. Fisk, F. Steglich, and S. Wirth, *Additional Energy Scale in* SmB₆ *at Low-Temperature*, Nat. Commun. **7**, 13762 (2016).

[23] L. Jiao and S. Rößler, D. Kasinathan, P. F. S. Rosa, C. Guo, H. Yuan, C.-X. Liu, Z. Fisk, F. Steglich, and S. Wirth, *Magnetic and Defect Probes of the* SmB₆ *Surface State*, Sci. Adv. **4**, eaau4886 (2018).

[24] H. Pirie, Y. Liu, A. Soumyanarayanan, P. Chen, Y. He, M. M. Yee, P. F. S. Rosa, J. D. Thompson, D.-J. Kim, Z. Fisk, X. Wang, J. Paglione, D. K. Morr, M. H. Hamidian, and J. E. Hoffman, *Imaging Emergent Heavy Dirac Fermions of a Topological Kondo Insulator*, Nat. Phys. **16**, 52 (2020).

[25] W. K. Park, L. Sun, A. Noddings, D.-J. Kim, Z. Fisk, and L. H. Greene, *Topological Surface States Interacting with Bulk Excitations in the Kondo Insulator* SmB₆ *Revealed via Planar Tunneling Spectroscopy*, Proc. Natl. Acad. Sci. U.S.A. **113**, 6599 (2016).

[26] W. K. Park, J. A. Sittler, L. H. Greene, W. T. Fuhrman, J. R. Chamorro, S. M. Koohpayeh, W. A. Phelan, and T. M. McQueen, *Topological Nature of the Kondo Insulator* SmB₆ *and Its Sensitiveness to Sm Vacancy*, Phys. Rev. B **103**, 155125 (2021).

[27] S. Wolgast, Ç. Kurdak, K. Sun, J. W. Allen, D.-J. Kim, and Z. Fisk, *Low-Temperature Surface Conduction in the Kondo Insulator* SmB₆, Phys. Rev. B **88**, 180405(R) (2013).

[28] D.-J. Kim, J. Xia, and Z. Fisk, *Topological Surface State in the Kondo Insulator Samarium Hexaboride*, Nat. Mater. **13**, 466 (2014).

[29] P. Hlawenka, K. Siemensmeyer, E. Weschke, A. Varykhalov, J. Sánchez-Barriga, N. Y. Shitsevalova, A. V. Dukhnenko, V. B. Filipov, S. Gabáni, K. Flachbart, O. Rader, and E. D. L. Rienks, *Samarium Hexaboride Is a Trivial Surface Conductor*, Nat. Commun. **9**, 517 (2018).

[30] M. Shahrokhvand, S. Pezzini, M. R. van Delft, U. Zeitler, N. E. Hussey, and S. Wiedmann, *Bulk and In-Gap States in* SmB₆ *Revealed by High-Field Magnetotransport*, Phys. Rev. B **96**, 205125 (2017).

[31] H. Weng, J. Zhao, Z. Wang, Z. Fang, and X. Dai, *Topological Crystalline Kondo Insulator in Mixed Valence Ytterbium Borides*, Phys. Rev. Lett. **112**, 016403 (2014).

[32] Y. Sato, Z. Xiang, Y. Kasahara, S. Kasahara, L. Chen, C. Tinsman, F. Iga, J. Singleton, N. L. Nair, N. Maksimovic, J. G. Analytis, Lu Li, and Y. Matsuda, *Topological Surface Conduction in Kondo Insulator* YbB₁₂, J. Phys. D **54**, 404002 (2021).

[33] K. Hagiwara, Y. Ohtsubo, M. Matsunami, S I. Ideta, K. Tanaka, H. Miyazaki, J. E. Rault, P. Le Fèvre, F. Bertran, A. Taleb-Ibrahimi, R. Yukawa, M. Kobayashi, K. Horiba, H. Kumigashira, K. Sumida, T. Okuda, F. Iga, and S. Kimura, *Surface Kondo Effect and Non-Trivial Metallic State of the Kondo Insulator* YbB₁₂, Nat. Commun. **7**, 12690 (2016).

[34] B. Tan, Y.-T. Hsu, B. Zeng, M. C. Hatnean, N. Harrison, Z. Zhu, M. Hartstein, M. Kiourlappou, A. Srivastava, M. D. Johannes, T. P. Murphy, J.-H. Park, L. Balicas, G. G. Lonzarich, G. Balakrishnan, and Suchitra E. Sebastian, *Unconventional Fermi Surface in an Insulating State*, Science **349**, 287 (2015).

[35] Z. Xiang, Y. Kasahara, T. Asaba, B. Lawson, C. Tinsman, L. Chen, K. Sugimoto, S. Kawaguchi, Y. Sato, G. Li, S. Yao, Y. L. Chen, F. Iga, J. Singleton, Y. Matsuda, and L. Li, *Quantum Oscillations of Electrical Resistivity in an Insulator*, Science **362**, 65 (2018).

[36] Z. Xiang, L. Chen, K.-W. Chen, C. Tinsman, Y. Sato, T. Asaba, H. Lu, Y. Kasahara, M. Jaime, F. Balakirev, F. Iga, Y. Matsuda, J. Singleton, and L. Li, *Unusual High-Field Metal in a Kondo Insulator*, Nat. Phys. **17**, 788 (2021).

[37] H. Liu, M. Hartstein, G. J. Wallace, A. J. Davies, M. Ciomaga Hatnean, M. D. Johannes, N. Shitsevalova, G. Balakrishnan, and S. E Sebastian, *Fermi Surfaces in*

Kondo Insulators, J. Phys. Condens. Matter **30,** 16LT01 (2018).

[38] M. Hartstein *et al.*, *Fermi Surface in the Absence of a Fermi Liquid in the Kondo Insulator* SmB$_6$, Nat. Phys. **14,** 166 (2018).

[39] Y. Sato, Z. Xiang, Y. Kasahara, T. Taniguchi, S. Kasahara, L. Chen, T. Asaba, C. Tinsman, H. Murayama, O. Tanaka, Y. Mizukami, T. Shibauchi, F. Iga, J. Singleton, L. Li, and Y. Matsuda, *Unconventional Thermal Metallic State of Charge-Neutral Fermions in an Insulator*, Nat. Phys. **15,** 954 (2019).

[40] G. Li, Z. Xiang, F. Yu, T. Asaba, B. Lawson, P. Cai, C. Tinsman, A. Berkley, S. Wolgast, Y. S. Eo, Dae-Jeong Kim, C. Kurdak, J. W. Allen, K. Sun, X. H. Chen, Y. Y. Wang, Z. Fisk, and Lu Li, *Two-Dimensional Fermi Surfaces in Kondo Insulator* SmB$_6$, Science **346,** 1208 (2014).

[41] Z. Xiang, B. Lawson, T. Asaba, C. Tinsman, Lu Chen, C. Shang, X. H. Chen, and L. Li, *Bulk Rotational Symmetry Breaking in Kondo Insulator* SmB$_6$, Phys. Rev. X **7,** 031054 (2017).

[42] S. M. Thomas, X. Ding, F. Ronning, V. Zapf, J. D. Thompson, Z. Fisk, J. Xia, and P. F. S. Rosa, *Quantum Oscillations in Flux-Grown* SmB$_6$ *with Embedded Aluminum*, Phys. Rev. Lett. **122,** 166401 (2019).

[43] Y. Xu, S. Cui, J. K. Dong, D. Zhao, T. Wu, X. H. Chen, K. Sun, H. Yao, and S. Y. Li, *Bulk Fermi Surface of Charge-Neutral Excitations in* SmB$_6$ *or Not: A Heat-Transport Study*, Phys. Rev. Lett. **116,** 246403 (2016).

[44] M.-E. Boulanger, F. Laliberté, M. Dion, S. Badoux, N. Doiron-Leyraud, W. A. Phelan, S. M. Koohpayeh, W. T. Fuhrman, J. R. Chamorro, T. M. McQueen, X. F. Wang, Y. Nakajima, T. Metz, J. Paglione, and L. Taillefer, *Field-Dependent Heat Transport in the Kondo Insulator* SmB$_6$: *Phonons Scattered by Magnetic Impurities*, Phys. Rev. B **97,** 245141 (2018).

[45] Lu Li, Kai Sun, Cagliyan Kurdak, and J. W. Allen, *Emergent Mystery in the Kondo Insulator Samarium Hexaboride*, Nat. Rev. Phys. **2,** 463 (2020).

[46] P. Coleman, E. Miranda, and A. Tsvelik, *Are Kondo Insulators Gapless?*, Physica (Amsterdam) **186B–188B,** 362 (1993).

[47] P. Coleman, E. Miranda, and A. Tsvelik, *Odd-Frequency Pairing in the Kondo Lattice*, Phys. Rev. B **49,** 8955 (1994).

[48] P. Coleman, L. B. Ioffe, and A. M. Tsvelik, *Simple Formulation of the Two-Channel Kondo Model*, Phys. Rev. B **52,** 6611 (1995).

[49] O. Erten, P.-Y. Chang, P. Coleman, and A. M. Tsvelik, *Skyrme Insulators: Insulators at the Brink of Superconductivity*, Phys. Rev. Lett. **119,** 057603 (2017).

[50] C. M. Varma, *Majoranas in Mixed-Valence Insulators*, Phys. Rev. B **102,** 155145 (2020).

[51] J. T. Heath and K. S. Bedell, *Universal Signatures of Majorana-like Quasiparticles in Strongly Correlated Landau-Fermi Liquids*, J. Phys. Condens. Matter **32,** 485602 (2020).

[52] I. Sodemann, D. Chowdhury, and T. Senthil, *Quantum Oscillations in Insulators with Neutral Fermi Surfaces*, Phys. Rev. B **97,** 045152 (2018).

[53] D. Chowdhury, I. Sodemann, and T. Senthil, *Mixed-Valence Insulators with Neutral Fermi-Surfaces*, Nat. Commun. **9,** 1766 (2018).

[54] P. Rao and I. Sodemann, *Cyclotron Resonance inside the Mott Gap: A Fingerprint of Emergent Neutral Fermions*, Phys. Rev. B **100,** 155150 (2019).

[55] O. I. Motrunich, *Orbital Magnetic Field Effects in Spin Liquid with Spinon Fermi Sea: Possible Application to* κ-ET$_2$Cu$_2$CN$_3$, Phys. Rev. B **72,** 045105 (2005).

[56] C. Putzke, S. Benhabib, W. Tabis, J. Ayres, Z. Wang, L. Malone, S. Licciardello, J. Lu, T. Kondo, T. Takeuchi, N. E. Hussey, J. R. Cooper, and A. Carrington, *Reduced Hall Carrier Density in the Overdoped Strange Metal Regime of Cuprate Superconductors*, Nat. Phys. **17,** 826 (2021).

[57] I. M. Hayes, N. Maksimovic, G. N. Lopez, M. K. Chan, B. J. Ramshaw, R. D. McDonald, and J. G. Analytis, *Superconductivity and Quantum Criticality Linked by the Hall Effect in a Strange Metal*, Nat. Phys. **17,** 58 (2021).

[58] M. Čulo, M. Berben, Y.-T. Hsu, J. Ayres, R. D. H. Hinlopen, S. Kasahara, Y. Matsuda, T. Shibauchi, and N. E. Hussey, *Putative Hall Response of the Strange Metal Component in* FeSe$_{1-x}$S$_x$, Phys. Rev. Research **3,** 023069 (2021).

[59] F. Iga, N. Shimizu, and T. Takabatake, *Single Crystal Growth and Physical Properties of Kondo Insulator* YbB$_{12}$, J. Magn. Magn. Mater. **177–181,** 337 (1998).

[60] Y. Luo, H. Chen, J. Dai, Z.-A. Xu, and J. D. Thompson, *Heavy Surface State in a Possible Topological Kondo Insulator: Magnetothermoelectric Transport on the (011) Plane of* SmB$_6$, Phys. Rev. B **91,** 075130 (2015).

[61] K. Sugiyama, F. Iga, M. Kasaya, T. Kasuya, and M. Date, *Field-Induced Metallic State in* YbB$_{12}$ *under High Magnetic Field*, J. Phys. Soc. Jpn. **57,** 3946 (1988).

[62] T. T. Terashima, A. Ikeda, Y. H. Matsuda, A. Kondo, K. Kindo, and F. Iga, *Magnetization Process of the Kondo Insulator* YbB$_{12}$ *in Ultrahigh Magnetic Fields*, J. Phys. Soc. Jpn. **86,** 054710 (2017).

[63] N. Nagaosa, J. Sinova, S. Onoda, A. H. MacDonald, and N. P. Ong, *Anomalous Hall Effect*, Rev. Mod. Phys. **82,** 1539 (2010).

[64] Y. Liu, H. Wang, H. Fu, J. Ge, Y. Li, C. Xi, J. Zhang, J. Yan, D. Mandrus, B. Yan, and J. Wang, *Induced Anomalous Hall Effect of Massive Dirac Fermions in* ZrTe$_5$ *and* HfTe$_5$ *Thin Flakes*, Phys. Rev. B **103,** L201110 (2021).

[65] Y.-X. Jiang *et al.*, *Unconventional Chiral Charge Order in Kagome Superconductor* KV$_3$Sb$_5$, Nat. Mater. **20,** 1353 (2021).

[66] P. Coleman, P. W. Anderson, and T. V. Ramakrishnan, *Theory for the Anomalous Hall Constant of Mixed-Valence Systems*, Phys. Rev. Lett. **55,** 414 (1985).

[67] A. Fert and P. M. Levy, *Theory of the Hall Effect in Heavy-Fermion Compounds*, Phys. Rev. B **36,** 1907 (1987).

[68] H. R. Naren, S. Friedemann, G. Zwicknagl, C. Krellner, C. Geibel, F. Steglich, and S. Wirth, *Lifshitz Transitions and Quasiparticle De-renormalization in* YbRh$_2$Si$_2$, New J. Phys. **15,** 093032 (2013).

[69] H. Pfau, R. Daou, S. Lausberg, H. R. Naren, M. Brando, S. Friedemann, S. Wirth, T. Westerkamp, U. Stockert,

P. Gegenwart, C. Krellner, C. Geibel, G. Zwicknagl, and F. Steglich, *Interplay between Kondo Suppression and Lifshitz Transitions in* $YbRh_2Si_2$ *at High Magnetic Fields,* Phys. Rev. Lett. **110,** 256403 (2013).

[70] Q. Niu, G. Knebel, D. Braithwaite, D. Aoki, G. Lapertot, M. Vališka, G. Seyfarth, W. Knafo, T. Helm, J.-P. Brison, J. Flouquet, and A. Pourret, *Evidence of Fermi Surface Reconstruction at the Metamagnetic Transition of the Strongly Correlated Superconductor* UTe_2, Phys. Rev. Research **2,** 033179 (2020).

[71] Y.-F. Yang, *Anomalous Hall Effect in Heavy Electron Materials,* Phys. Rev. B **87,** 045102 (2013).

[72] C. M. Hurd, *The Hall Effect in Metals and Alloys* (Plenum Press, New York, 1972).

[73] N. P. Ong, *Geometric Interpretation of the Weak-Field Hall Conductivity in Two-Dimensional Metals with Arbitrary Fermi Surface,* Phys. Rev. B **43,** 193 (1991).

[74] Y. Nakajima, K. Izawa, Y. Matsuda, K. Behnia, H. Kontani, M. Hedo, Y. Uwatoko, T. Matsumoto, H. Shishido, R. Settai, and Y. Onuki, *Evolution of Hall Coefficient in Two-Dimensional Heavy Fermion* $CeCoIn_5$, J. Phys. Soc. Jpn. **75,** 023705 (2006).

[75] Y. Nakajima, H. Shishido, H. Nakai, T. Shibauchi, K. Behnia, K. Izawa, M. Hedo, Y. Uwatoko, T. Matsumoto, R. Settai, Y. Onuki, H. Kontani, and Y. Matsuda, *Non-Fermi Liquid Behavior in the Magnetotransport of Ce* MIn_5 *(M: Co and Rh): Striking Similarity between Quasi Two-Dimensional Heavy Fermion and High-T_c Cuprates,* J. Phys. Soc. Jpn. **76,** 024703 (2007).

[76] J.-M. Mignot, P. A. Alekseev, K. S. Nemkovski, L.-P. Regnault, F. Iga, and T. Takabatake, *Evidence for Short-Range Antiferromagnetic Fluctuations in Kondo-Insulating* YbB_{12}, Phys. Rev. Lett. **94,** 247204 (2005).

[77] A. Akbari, P. Thalmeier, and P. Fulde, *Theory of Spin Exciton in the Kondo Semiconductor* YbB_{12}, Phys. Rev. Lett. **102,** 106402 (2009).

[78] G. A. Kapilevich, P. S. Riseborough, A. X. Gray, M. Gulacsi, T. Durakiewicz, and J. L. Smith, *Incomplete Protection of the Surface Weyl Cones of the Kondo Insulator* SmB_6: *Spin Exciton Scattering,* Phys. Rev. B **92,** 085133 (2015).

[79] W. K. Huang, S. Hosoi, M. Čulo, S. Kasahara, Y. Sato, K. Matsuura, Y. Mizukami, M. Berben, N. E. Hussey, H. Kontani, T. Shibauchi, and Y. Matsuda, *Non-Fermi Liquid Transport in the Vicinity of the Nematic Quantum Critical Point of Superconducting* $FeSe_{1-x}S_x$, Phys. Rev. Research **2,** 033367 (2020).

[80] S. Kasahara, T. Shibauchi, K. Hashimoto, K. Ikada, S. Tonegawa, R. Okazaki, H. Shishido, H. Ikeda, H. Takeya, K. Hirata, T. Terashima, and Y. Matsuda, *Evolution from Non-Fermi- to Fermi-Liquid Transport via Isovalent Doping in* $BaFe_2(As_{1-x}P_x)_2$ *Superconductors,* Phys. Rev. B **81,** 184519 (2010).

[81] T. Shibauchi, A. Carrington, and Y. Matsuda, *A Quantum Critical Point Lying beneath the Superconducting Dome in Iron Pnictides,* Annu. Rev. Condens. Matter Phys. **5,** 113 (2014).

[82] T. T. Terashima, Y. H. Matsuda, Y. Kohama, A. Ikeda, A. Kondo, K. Kindo, and F. Iga, *Magnetic-Field-Induced Kondo Metal Realized in* YbB_{12}, Phys. Rev. Lett. **120,** 257206 (2018).

[83] I. M. Lifshitz, *Anomalies of Electron Characteristics of a Metal in the High Pressure Region,* Zh. Eksp. Teor. Fiz. **38,** 1569 (1960) [Sov. Phys. JETP **11,** 1130 (1960)].

[84] K. S. D. Beach, P. A. Lee, and P. Monthoux, *Field-Induced Antiferromagnetism in the Kondo Insulator,* Phys. Rev. Lett. **92,** 026401 (2004).

[85] T. Ohashi, A. Koga, S. Suga, and N. Kawakami, *Field-Induced Phase Transitions in a Kondo Insulator,* Phys. Rev. B **70,** 245104 (2004).

[86] D. Aoki, G. Seyfarth, A. Pourret, A. Gourgout, A. McCollam, J. A. N. Bruin, Y. Krupko, and I. Sheikin, *Field-Induced Lifshitz Transition without Metamagnetism in* $CeIrIn_5$, Phys. Rev. Lett. **116,** 037202 (2016).

[87] S. Viola Kusminskiy, K. S. D. Beach, A. H. Castro Neto, and D. K. Campbell, *Mean-Field Study of the Heavy-Fermion Metamagnetic Transition,* Phys. Rev. B **77,** 094419 (2008).

[88] A. Pourret, S. G. Sharapov, T. D. Matsuda, G. Knebel, G. Zwicknagl, and A. A. Varlamov, *Transport Spectroscopy of the Field Induced Cascade of Lifshitz Transitions in* $YbRh_2Si_2$, J. Phys. Soc. Jpn. **88,** 104702 (2019).

[89] H. Pfau, R. Daou, S. Friedemann, S. Karbassi, S. Ghannadzadeh, R. Küchler, S. Hamann, A. Steppke, D. Sun, M. König, A. P. Mackenzie, K. Kliemt, C. Krellner, and M. Brando, *Cascade of Magnetic-Field-Induced Lifshitz Transitions in the Ferromagnetic Kondo Lattice Material* $YbNi_4P_2$, Phys. Rev. Lett. **119,** 126402 (2017).

[90] P. M. C. Rourke, A. McCollam, G. Lapertot, G. Knebel, J. Flouquet, and S. R. Julian, *Magnetic-Field Dependence of the* $YbRh_2Si_2$ *Fermi Surface,* Phys. Rev. Lett. **101,** 237205 (2008).

[91] H. Aoki, N. Kimura, and T. Terashima, *Fermi Surface Properties, Metamagnetic Transition and Quantum Phase Transition of* $CeRu_2Si_2$ *and Its Alloys Probed by the dHvA Effect,* J. Phys. Soc. Jpn. **83,** 072001 (2014).

[92] D. Shoenberg, *Magnetic Oscillations in Metals,* (Cambridge University Press, Cambridge, England, 2009).

[93] See Supplemental Material at http://link.aps.org/supplemental/10.1103/PhysRevX.12.021050 for further supporting data and discussions on the crystal electric field levels in YbB_{12}.

[94] D. Chattopadhyay and H. J. Queisser, *Electron Scattering by Ionized Impurities in Semiconductors,* Rev. Mod. Phys. **53,** 745 (1981).

[95] P. A. Lee and T. V. Ramakrishnan, *Disordered Electronic System,* Rev. Mod. Phys. **57,** 287 (1985).

[96] Ya. I. Rodionov and S. V. Syzranov, *Conductivity of a Weyl Semimetal with Donor and Acceptor Impurities,* Phys. Rev. B **91,** 195107 (2015).

[97] S. Das Sarma, E. H. Hwang, and H. Min, *Carrier Screening, Transport, and Relaxation in Three-Dimensional Dirac Semimetals,* Phys. Rev. B **91,** 035201 (2015).

[98] Ya. I. Rodionov, K. I. Kugel, B. A. Aronzon, and F. Nori, *Effect of Disorder on the Transverse Magnetoresistance of Weyl Semimetals,* Phys. Rev. B **102,** 205105 (2020).

[99] H. Shen and L. Fu, *Quantum Oscillation from In-Gap States and Non-Hermitian Landau Level Problem,* Phys. Rev. Lett. **121,** 026403 (2018).

[100] N. Harrison, *Highly Asymmetric Nodal Semimetal in Bulk* SmB$_6$, Phys. Rev. Lett. **121,** 026602 (2018).

[101] A. W. Sleight and A. P. Ramirez, *Disappearance of the Metal-Insulator Transition in Iridate Pyrochlores on Approaching the Ideal* R$_2$Ir$_2$O$_7$ *Stoichiometry,* Solid State Commun. **275,** 12 (2018).

[102] P. G. LaBarre, L. Dong, J. Trinh, T. Siegrist, and A. P. Ramirez, *Evidence for Undoped Weyl Semimetal Charge Transport in* Y$_2$Ir$_2$O$_7$, J. Phys. Condens. Matter **32,** 02LT01 (2020).

[103] A. B. Pippard, *Magnetoresistance in Metals* (Cambridge University Press, Cambridge, England, 1989).

[104] E. N. Adams and T. D. Holstein, *Quantum Theory of Transverse Galvano-Magnetic Phenomena,* J. Phys. Chem. Solids **10,** 254 (1959).

[105] F. E. Richards, *Investigation of the Magnetoresistance Quantum Oscillations in Magnesium,* Phys. Rev. B **8,** 2552 (1973).

[106] W. G. Baber, *The Contribution to the Electrical Resistance of Metals from Collisions between Electrons,* Proc. R. Soc. A **158,** 383 (1937).

[107] Considering the size of neutral Fermi surface revealed by SdH frequency ($F \simeq 700$ T, consistent with a Fermi vector $k_F \simeq 1.46$ nm^{-1}, i.e., approximately $0.18(2\pi/a)$, $a = 7.47$ Å is the lattice constant [36]), and the relatively low density of charge carriers in the KI state, the conventional Umklapp event should be ineffective in YbB$_{12}$ since it requires a k_F longer than one fourth the size of the smallest vector of the reciprocal lattice [108]. Additionally, the fact that the scattering appears to be strong even at the lowest temperatures (corroborated by the saturating SdH amplitudes toward $T = 0$ [93]), the involvement of phonons in the scattering process can be generally excluded.

[108] X. Lin, B. Fauqué, and K. Behnia, *Scalable T^2 Resistivity in a Small Single-Component Fermi Surface,* Science **349,** 945 (2015).

[109] S. R. Park, W. S. Jung, Chul Kim, D. J. Song, C. Kim,1, S. Kimura, K. D. Lee, and N. Hur, *Quasiparticle Scattering and the Protected Nature of the Topological States in a Parent Topological Insulator* Bi$_2$Se$_3$, Phys. Rev. B **81,** 041405(R) (2010).

[110] C. J. Lin, X. Y. He, J. Liao, X. X. Wang, V. Sacksteder, W. M. Yang, T. Guan, Q. M. Zhang, L. Gu, G. Y. Zhang, C. G. Zeng, X. Dai, K. H. Wu, and Y. Q. Li, *Parallel Field Magnetoresistance in Topological Insulator Thin Films,* Phys. Rev. B **88,** 041307(R) (2013).

[111] Y. Yuan, X. Yang, L. Peng, Z.-J. Wang, J. Li, C.-J. Yi, J.-J. Xian, Y.-G. Shi, and Y.-S. Fu, *Quasiparticle Interference of Fermi Arc States in the Type-II Weyl Semimetal Candidate* WTe$_2$, Phys. Rev. B **97,** 165435 (2018).

[112] V. Alexandrov, P. Coleman, and O. Erten, *Kondo Breakdown in Topological Kondo Insulators,* Phys. Rev. Lett. **114,** 177202 (2015).

[113] G. G. Lesseux, H. Sakai, T. Hattori, Y. Tokunaga, S. Kambe, P. L. Kuhns, A. P. Reyes, J. D. Thompson, P. G. Pagliuso, and R. R. Urbano, *Orbitally Defined Field-Induced Electronic State in a Kondo Lattice,* Phys. Rev. B **101,** 165111 (2020).

[114] R. Kurihara, A. Miyake, M. Tokunaga, A. Ikeda, Y. H. Matsuda, A. Miyata, D. I. Gorbunov, T. Nomura, S. Zherlitsyn, J. Wosnitza, and F. Iga, *Field-Induced Valence Fluctuations in* YbB$_{12}$, Phys. Rev. B **103,** 115103 (2021).

[115] J. Knolle and N. R. Cooper, *Quantum Oscillations without a Fermi Surface and the Anomalous de Haas–van Alphen Effect,* Phys. Rev. Lett. **115,** 146401 (2015).

[116] A. A, Allocca, and N. R. Cooper, *Quantum Oscillations in Interaction-Driven Insulators,* SciPost Phys. **12,** 123 (2022).

[117] J. Knolle and N. R. Cooper, *Excitons in Topological Kondo Insulators: Theory of Thermodynamic and Transport Anomalies in* SmB$_6$, Phys. Rev. Lett. **118,** 096604 (2017).

[118] L. Zhang, X.-Y. Song, and F. Wang, *Quantum Oscillation in Narrow-Gap Topological Insulators,* Phys. Rev. Lett. **116,** 046404 (2016).

[119] H. K. Pal, F. Piéchon, J.-N. Fuchs, M. Goerbig,1, and G. Montambaux, *Chemical Potential Asymmetry and Quantum Oscillations in Insulators,* Phys. Rev. B **94,** 125140 (2016).

[120] S. Grubinskas and L. Fritz, *Modification of the Lifshitz-Kosevich Formula for Anomalous de Haas–van Alphen Oscillations in Inverted Insulators,* Phys. Rev. B **97,** 115202 (2018).

[121] R. Peters, T. Yoshida, and N. Kawakami, *Quantum Oscillations in Strongly Correlated Topological Kondo Insulators,* Phys. Rev. B **100,** 085124 (2019).

[122] Y. Tada, *Cyclotron Resonance in Kondo Insulator,* Phys. Rev. Research **2,** 023194 (2020).

[123] Y.-W. Lu, P.-H. Chou, C.-H. Chung, T.-K. Lee, and C.-Y. Mou, *Enhanced Quantum Oscillations in Kondo Insulators,* Phys. Rev. B **101,** 115102 (2020).

[124] H. K. Pal, *Quantum Oscillations from inside the Fermi Sea,* Phys. Rev. B **95,** 085111 (2017).

[125] H. Liu, A. J. Hickey, M. Hartstein, A. J. Davies, A. G. Eaton, T. Elvin, E. Polyakov, T. H. Vu, V. Wichitwechkarn, T. Förster, J. Wosnitza, T. P. Murphy, N. Shitsevalova, M. D. Johannes, M. Ciomaga Hatnean, G. Balakrishnan, G. G. Lonzarich, and S. E. Sebastian, *f-Electron Hybridised Fermi Surface in Magnetic Field-Induced Metallic* YbB$_{12}$, npj Quantum Mater. **7,** 12 (2022).

[126] P. Schlottmann and C. S. Hellberg, *Metal-Insulator Transition in Dirty Kondo Insulators,* J. Appl. Phys. **79,** 6414 (1996).

[127] B. Skinner, *Properties of the Donor Impurity Band in Mixed Valence Insulators,* Phys. Rev. Mater. **3,** 104601 (2019).

[128] S. Sen, N. S. Vidhyadhiraja, E. Miranda, V. Dobrosavljević, and W. Ku, *Fragility of the Kondo Insulating Gap against Disorder: Relevance to Recent Puzzles in Topological Kondo Insulators,* Phys. Rev. Research **2,** 033370 (2020).

[129] W. T. Fuhrman and P. Nikolić, *Magnetic Impurities in Kondo Insulators: An Application to Samarium Hexaboride,* Phys. Rev. B **101,** 245118 (2020).

[130] M. Pickem, E. Maggio, and J. M. Tomczak, *Resistivity Saturation in Kondo Insulators,* Commun. Phys. **4,** 226 (2021).

[131] Y. S. Eo, A. Rakoskia, J. Luciena, and D. Mihaliova, Ç. Kurdak, P. F. S. Rosa, and Z. Fisk, *Transport Gap in* SmB$_6$ *Protected against Disorder*, Proc. Natl. Acad. Sci. U.S.A. **116**, 12638 (2019).

[132] M. N. Ali, J. Xiong, S. Flynn, J. Tao, Q. D. Gibson, L. M. Schoop, T. Liang, N. Haldolaarachchige, M. Hirschberger, N. P. Ong, and R. J. Cava, *Large, Non-Saturating Magnetoresistance in* WTe$_2$, Nature (London) **514**, 205 (2014).

[133] N. W. Ashcroft and N. David Mermin, *Solid State Physics* (Harcourt, Orlando, 1976).

[134] J. S. Kim, *A Matrix Formalism for the Hall Effect in Multicarrier Semiconductor System*, J. Appl. Phys. **86**, 3187 (1999).

[135] P. M. C. Rourke, A. F. Bangura, C. Proust, J. Levallois, N. Doiron-Leyraud, D. LeBoeuf, L. Taillefer, S. Adachi, M. L. Sutherland, and N. E. Hussey, *Fermi-Surface Reconstruction and Two-Carrier Model for the Hall Effect in* YBa$_2$Cu$_4$O$_8$, Phys. Rev. B **82**, 020514(R) (2010).

[136] D. Schulze Grachtrup, N. Steinki, S. Süllow, Z. Cakir, G. Zwicknagl, Y. Krupko, I. Sheikin, M. Jaime, and J. A. Mydosh, *Magnetic Phase Diagram and Electronic Structure of* UPt$_2$Si$_2$ *at High Magnetic Fields: A Possible Field-Induced Lifshitz Transition*, Phys. Rev. B **95**, 134422 (2017).